
Politecnico di Torino


# Politecnico di Torino

## Dipartimento di Ingegneria Meccanica e Aerospaziale


Master's Degree in Aerospace Engineering

Academic Year: 2023/2024

Graduation session: October 2024

# FLIGHT PATH RECONSTRUCTION ON FLIGHT TEST DATA OF A LIGHTWEIGHT HELICOPTER


Supervisors:

Prof. Giorgio Guglieri
Prof. Pierluigi Capone
Anna Abà

Candidate:

Michele Cosimo Ladu

# Abstract

This thesis aims to describe the Flight Path Reconstruction (FPR) process based on flight test data of a new lightweight, multi-purpose helicopter. FPR is a procedure that must be performed during the system identification process to increase the quality of measured data and ensure a more reliable aerodynamic parameter estimation. The thesis aims to determine an error model for several aerodynamic sensors by comparing the measured aerodynamic parameters with the reconstructed flow angles.

The first phase of the project involved pre-processing the available flight test data. First, it was necessary to select which signals, among all that were recorded, were of interest to the project. Subsequently, those signals have been converted into MATLAB tables as all the scripts used are written in MATLAB language. Some signals required additional conversion as they were coded in ARINC 429 protocol. The next step of the work involved slicing data from every flight into single manoeuvres, these were then categorised based on the type, speed and altitude.

The second part of the thesis focuses on Flight Path Reconstruction, a lengthy and iterative process that makes extensive use of the Output Error Method.

The project was conducted during an exchange program at ZHAW (Zurich University of Applied Sciences) in Winterthur, Switzerland, from April to June 2024. This thesis is part of a wider project whose main goal is to develop a high-fidelity simulation model.

# Aknowledgments

I want to express my deepest gratitude to Professor Giorgio Guglieri of Politecnico di Torino, for giving me the opportunity to complete my master's degree in such a stimulating and interesting project. I'm also grateful to the Zürich University of Applied Sciences for the support during my stay in Winterthur, especially to Professor Pierluigi Capone, Anna Abà and the entire Flight Mechanics team of the Centre for Aviation for the help and guidance that made this thesis possible.

October, 2024 Michele Cosimo Ladu

# Contents

# List of Figures

# List of Tables

# List of Symbols

**Greek alphabet**

| | |
|---|---|
| $\alpha$ | Angle of Attack |
| $\beta$ | Angle of Sideslip |
| $\gamma$ | Isoentropic expansion coefficient |
| $[\phi, \theta, \psi]$ | Euler angles |
| $[\dot{\phi}, \dot{\theta}, \dot{\psi}]$ | Euler angles derivatives |
| $\rho$ | Air density |

**Latin alphabet**

| | |
|---|---|
| $[\dot{p}, \dot{q}, \dot{r}]$ | Angular rates derivatives |
| $[\dot{u}, \dot{v}, \dot{w}]$ | Velocity components derivatives |
| $[a_x, a_y, a_z]$ | Acceleration components |
| $[p, q, r]$ | Angular rates |
| $[u, v, w]$ | Velocity components |
| $\bar{q}$ | Dynamic pressure |
| $\dot{h}$ | Altitude derivative |
| $h$ | Altitude |
| $M$ | Mach number |
| $R$ | Gas constant |
| $T$ | Air temperature |

### Abbreviations

| | |
|---|---|
| ADAHRS | Air Data Attitude Heading Reference System |
| ADB | Air Data Boom |
| AoA | Angle of Attack |
| AoB | Angle of Bank |
| AoS | Angle of Sideslip |
| CAS | Calibrated Airspeed |
| DLR | Deutsches Zentrum für Luft- und Raumfahrt |
| DoF | Degree of Freedom |
| EKF | Extended Kalman Filter |
| ESIS | Electronic Standby Instrument System |
| FPR | Flight Path Reconstruction |
| FS | Full Scale |
| MoI | Moment of Inertia |
| OEM | Output Error Method |
| PoI | Product of Inertia |
| TAS | True Airspeed |
| VRU | Vertical Reference Unit |
| WHeSI | White-box Helicopter System Identification |
| ZAV | Zentrum für Aviatik (Centre for Aviation) |
| ZHAW | Zürcher Hochschule für Angewandte Wissenschaften (Zurich University of Applied Sciences) |

### Subscripts

| | |
|---|---|
| c | corrected |
| m | measured |
| r | reconstructed |

# Chapter 1

# Introduction

## 1.1 WHeSI

The WHeSI (White-box Helicopter System Identification) project is a collaboration between the Swiss helicopter manufacturer Kopter and the Centre for Aviation (ZAV) of the Zurich University of Applied Sciences (ZHAW). The project's scope is to develop a high-fidelity simulation model of *Kopter*'s brand new helicopter, *AW09*.

The model will then be used to support the rotorcraft's design and certification, reducing the time and costs associated with flight testing. In order to achieve the fidelity level required for such an application, a fully physics-based, non-linear model is required, whose parameters are estimated with an innovative time domain system identification approach [9].

The thesis is the result of the work done in collaboration with the flight mechanics department of the ZAV within the framework of this project.

## 1.2 Thesis scope

Aircraft system identification is a lengthy and complex process. Starting from raw flight test data, several steps must be completed to check for any incompatibility between the recorded signals [1]. This enables us to increase the data quality and check for any errors that could invalidate subsequent analyses, mainly, parameter estimation.

One technique, called Data Compatibility Check or Flight Path Reconstruction (FPR), consists of comparing the measured aerodynamic signals with the flow angles obtained from the numerical integration of a set of kinematic equations. The inputs of these equations are the signals recorded by the inertial measurement unit, considered more reliable than the aerodynamic signals. This comparison enables

us to determine any systematic instrument error of the aerodynamic sensors [2].

The scope of this master's thesis is to perform a preliminary Flight Path Reconstruction on the data obtained in several flight tests conducted during 2024. The FPR framework of the ZAV was already tested for fixed-wing aircraft during previous theses ([3] and [4]), this work aims to adapt and update the existing framework to the new rotary-wing project.

The end goal of the thesis is to obtain an estimate of the error models of the aerodynamic sensors mounted on the helicopter. The results obtained from the work will then be used as a starting point for a more detailed flight path reconstruction on future flight test campaigns.

# Chapter 2

# Test Aircraft and instrumentation

## 2.1 *Kopter AW09*

*Kopter's AW09* is an innovative single-engine helicopter capable of carrying up to 8 passengers and 1 pilot, thanks to its composite structure it has a Maximum Take-Off Weight of about 3000 kg. The light weight, combined with the single turbine engine, results in remarkable performances in terms of range and endurance as reported in table 2.1. The mounted engine is the *Safran Arriel 2K* turbine engine, capable of producing 1000 shaft horsepower, the propulsive system also features a dual channel FADEC system for improved performance and engine monitoring. Noise levels and vibrations are reduced thanks to the 5-blade composite main rotor and the 10-blade shrouded tail rotor, which also increases safety during ground operations. The avionic system is of the latest generation with a full glass cockpit equipped with *Garmin G3000H*. The *AW09* is suited for a broad range of missions, such as utility, passenger transport, Emergency Medical Services and security. The modular design of the cabin allows for quick conversion from one configuration to another [10][11].

The aircraft involved in the flight test campaign from which all the data was derived is registration HB-ZXD, based in Mollis airport in the Canton of Glarus, Switzerland (figure 2.1).

## 2.2 Flight Test Instrumentation

### 2.2.1 Air Data Boom

Aerodynamic signals were measured through an Air Data Boom (ADB) attached to the cockpit structure on the lower front part. The positioning allows to obtain measurements not affected by the downwash of the main rotor, especially during


Figure 2.1: Test helicopter HB-ZXD [*Kopter*]

forward flight when the rotor wake is transported backwards by the relative wind.

A standard 5-hole probe measures static and total air pressure, as well as the differential pressures needed for the computation of the Angle of Attack and the Angle of Sideslip. A separate sensor measures the Total Air Temperature. The raw data is then fed to a microprocessor that computes the aircraft's altitude, airspeed and rate of climb. Table 2.2 describes the ranges and accuracies of the Air Data Boom.

The ADB assembly can be seen in figure 2.2. The probe is mounted at the end of a supporting structure connected to the cockpit through an adjustable bracket, allowing for incidence variation. Two lateral rods support the main one maintaining the probe in the symmetry plane of the helicopter.

### 2.2.2 Inertial Measurement Unit

Linear accelerations, rotational rates and Euler angles were measured by the IMU of the ADAHRS unit, located almost in the symmetry plane of the helicopter. Other inertial measurements were collected for comparison from the Electric Standby Instrumentation System and the Garmin equipment.


Figure 2.2: Air Data Boom assembly [*Leonardo*]

| Feature | Value | Unit |
|---|---|---|
| Length | 13.3 | m |
| Height | 3.74 | m |
| Rotor diameter | 10.96 | m |
| MTOW | 2850 | kg |
| MTOW with external load | >3000 | kg |
| Power | 750 | kW |
| Range | 800 | km |
| Endurance | 5 | h |
| Maximum speed | 260 | km/h |
| Capacity | 8+1 | - |

Table 2.1: Summary table of AW09 characteristics

| Parameter | Range | Unit | Accuracy |
|---|---|---|---|
| Static pressure | 238-1080 | hPa | $< 0.2\%$ FS |
| Calibrated Airspeed | $< 350$ | kn | $< 0.5\%$ FS |
| Angle of Attack | $\pm 25$ | $^\circ$ | $< 0.5^\circ$ |
| Angle of Sideslip | $\pm 25$ | $^\circ$ | $< 0.5^\circ$ above 60 kn CAS<br>$< 0.3^\circ$ above 100 kn CAS |

Table 2.2: Air Data Boom characteristics

# Chapter 3

# Theoretical background

## 3.1 System Identification

In the broad realm of the mathematical modelling problem, system identification is the discipline that aims to obtain a model of the real physical system based on measured inputs and outputs of the system itself. The goal of the identification process is to obtain a mathematical model of the physical system, usually written as:

$$\begin{cases} \dot{x} = f(x(t), u(t)|\Theta) \\ y = g(x(t), u(t)|\Theta) \end{cases} \tag{3.1}$$

where $x$, $y$ and $u$ are the state, output and input vectors respectively, $f$ and $g$ are the mathematical functions and $\Theta$ is the unknown parameter vector.

Mathematical models can be classified into white-box or behavioural models and black-box or phenomenological models, the term grey-box model is often used when the two approaches are combined. Behavioural models are derived from the system's physics and result in a set of differential equations whose parameters represent the system's real physical characteristics. Phenomenological models instead describe the system's behaviour as a set of cause-effect relationships and the system parameters are not related to any physical entity.

Once the mathematical model is obtained, the unknown parameters $\Theta$ can be estimated by comparing the measurements $z$ (from the real system) with the outputs $y$, computed by numerical simulation of the mathematical model given the inputs $u$. Depending on the fidelity level of the model and the errors affecting the measurements, $z$ and $y$ are different to some extent as a perfect correspondence is impossible.

After parameter estimation, the model must be validated to determine if the requirements are met, if not, the process must be repeated [2].

### 3.1.1 Aircraft system identification

In the aeronautical sector, mathematical modelling is used during the design and certification phases of the project, as well as during training. Time, costs and risks associated with these processes are greatly reduced if an adequate level of modelling and simulation is involved.

When applied to fixed-wing and rotary-wing vehicles, the system identification framework integrates the following three disciplines [2] [5]:

- instrumentation and filters needed to acquire flight data;
- flight test techniques aimed at exciting all the aircraft's dynamic response modes;
- analysis of flight test data to accurately estimate the aircraft parameters.

The so-called 'Quad-M' requirements are then defined (figure 3.2):

- the input time history must be adequate to excite all modes of the aircraft's dynamic **M**otion;
- the type of the aircraft must be studied to define the structure of the mathematical **M**odel;
- instrumentation and filters must produce high-quality **M**easurements;
- data analysis must be done through proper identification **M**ethods.

## 3.2 Data compatibility check

The availability of good quality flight test data is crucial to perform a successful aircraft parameter estimation. First, the flight test campaign must be carefully planned to enable the extraction of the maximum amount of data from the least

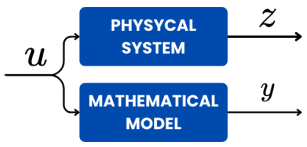


Figure 3.1: System identification scheme, based on [2]

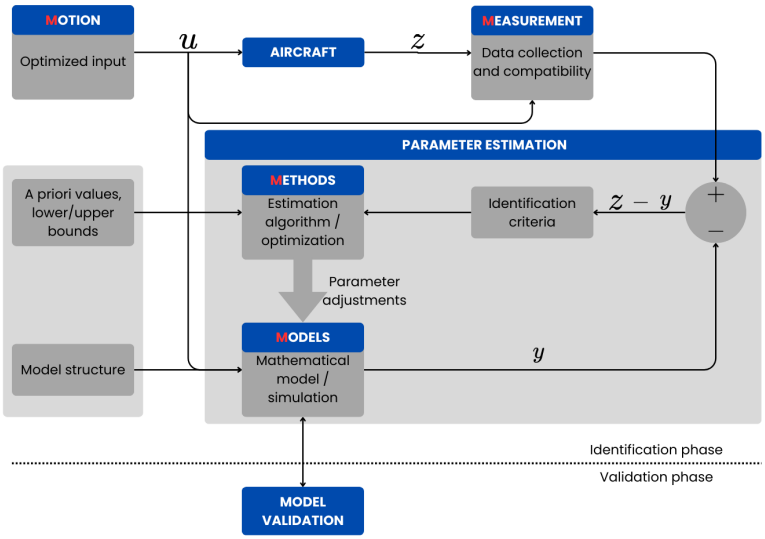


Figure 3.2: 'Quad-M' architecture, based on [2]

amount of flying hours, reducing at the same time costs and risks associated with testing. The instrumentation must be correctly installed, calibrated and tested beforehand, to ensure that the data is affected by the minimum amount of corruption possible. During the tests, the flight crew must perform a predetermined set of manoeuvres with adequate input signals, while the engineers must check the data for any problem that may arise and invalidate the tests. A visual inspection of the data plots is always performed after each flight to spot any major issues, like wrong sign conventions, data dropouts and excessive noise levels that could indicate the deterioration of the flight test instrumentation.

After the test campaign is over, compatibility checking aims to improve the quality of the data by exploiting the redundancy of measurements of the same variable. The goal is to determine if any systematic errors, like scale factors, time delays and sensor biases, are present in the measurement instruments. In particular, aerodynamic variables are compared to the ones reconstructed from the integration of the kinematic equations of motion to determine the aerodynamic sensors' error models. This process is called kinematic compatibility checking (or Flight Path Reconstruction).

### 3.2.1 Kinematic compatibility checking

Aerodynamic sensors have been historically affected by errors of much greater magnitude than inertial sensors. Starting from measured linear accelerations and rotational rates, it is possible to integrate the aircraft kinematic equations of motion (equation 3.2) and reconstruct the aerodynamic variables.

$$\begin{cases} \dot{u} = (rv - qw) - g\sin\theta + a_x \\ \dot{v} = (pw - ru) + g\sin\phi\cos\theta + a_y \\ \dot{w} = (qu - pv) + g\cos\phi\cos\theta + a_z \\ \dot{p} = -\frac{J_z - J_y}{J_x} qr + \frac{L}{J_x} \\ \dot{q} = -\frac{J_x - J_z}{J_y} pr + \frac{M}{J_y} \\ \dot{r} = -\frac{J_y - J_x}{J_z} pq + \frac{N}{J_z} \\ \dot{\phi} = p + q\sin\phi\tan\theta + r\cos\phi\tan\theta \\ \dot{\theta} = q\cos\phi - r\sin\phi \\ \dot{\psi} = q\frac{\sin\phi}{\cos\theta} + r\frac{\cos\phi}{\cos\theta} \\ \dot{x} = u\cos\psi\cos\theta + v(\cos\psi\sin\theta\sin\phi - \sin\psi\cos\theta) + \\ \qquad + w(\cos\psi\sin\theta\cos\phi + \sin\psi\sin\phi \\ \dot{y} = u\sin\psi\cos\theta - v(\sin\psi\sin\theta\sin\phi - \cos\psi\cos\phi) + \\ \qquad + w(\sin\psi\sin\theta\cos\phi - \cos\psi\sin\phi) \\ \dot{h} = -u\sin\theta + v\cos\theta\sin\phi + w\cos\theta\cos\phi \end{cases} \tag{3.2}$$

In detail, the measurements of the rotational rates $(p, q, r)$ and the linear accelerations $(a_x, a_y, a_z)$ obtained by the IMU are used to reconstruct the flow velocities $(u, v, w)$, the Euler angles $(\phi, \theta, \psi)$ and the position of the aircraft $(x, y, h)$. The state vector must be initialised, either from actual measurements or state estimation. The navigation equations for $\dot{x}$ and $\dot{y}$ are decoupled and can be omitted for simplicity. This was also done because the GNSS measurements were unreliable and therefore it was impossible to compare the reconstructed position with the actual one.

Once the state vector is derived, the aerodynamic variables are computed through:

$$\begin{aligned} V &= \sqrt{u^2 + v^2 + w^2} \\ \alpha &= \arctan\frac{w}{u} \\ \beta &= \arcsin\frac{v}{V} \\ \bar{q} &= \frac{1}{2}\rho V^2 \end{aligned} \tag{3.3}$$

where:

- $V$ is the airspeed;
- $\alpha$ is the angle of attack (AoA);
- $\beta$ is the angle of sideslip (AoS);
- $\bar{q}$ is the dynamic pressure.
- $\rho$ is the air density, computed from static pressure $p_\mathrm{s}$ and static temperature $T_\mathrm{s}$:

$$\rho = \frac{p_\mathrm{s}}{RT_\mathrm{s}} \tag{3.4}$$

For each aerodynamic variable, a sensor error model can be written [2]:

$$y_\mathrm{m} = K_y(t-\tau)\cdot y + b_y \tag{3.5}$$

where the subscript "m" stands for "measured" and:

- $K_y$ is the scale factor;
- $\tau$ is the time delay;
- $b_y$ is the bias.

The goal of FPR is to find a value for these parameters that is valid throughout the entire aircraft envelope. However, the results of FPR are subject to the test data itself, so the error models will be dependent on the manoeuvres performed during the test campaign. In this thesis, the time delay $\tau$ is assumed to be negligible for the studied sensors and therefore will not be estimated.

Returning briefly to the state estimation, some assumptions and corrections must be made. Flow velocities $(u, v, w)$ are estimated from linear accelerations $(a_x, a_y, a_z)$ and rotational rates $(p, q, r)$. However, this is true only if we assume that the wind is constant both in direction and magnitude as these variables are defined in the two different reference frames: aerodynamic for $(u, v, w)$ and inertial for $(a_x, a_y, a_z)$ and $(p, q, r)$. Furthermore, linear accelerations must be computed at the centre of gravity (CoG) as they are measured at the IMU:

$$\begin{cases} a_{x,\mathrm{CoG}} = a_{x\mathrm{m,IMU}} + (q^2+r^2)d_{x,\mathrm{IMU}} + (pq-\dot{r})d_{y,\mathrm{IMU}} - (pr+\dot{q})d_{z,\mathrm{IMU}} \\ a_{y,\mathrm{CoG}} = a_{y\mathrm{m,IMU}} - (pq+\dot{r})d_{x,\mathrm{IMU}} + (p^2+r^2)d_{y,\mathrm{IMU}} - (qr-\dot{p})d_{z,\mathrm{IMU}} \\ a_{z,\mathrm{CoG}} = a_{z\mathrm{m,IMU}} + (pr-\dot{q})d_{x,\mathrm{IMU}} + (qr+\dot{p})d_{y,\mathrm{IMU}} - (p^2+q^2)d_{z,\mathrm{IMU}} \end{cases} \tag{3.6}$$

where $(d_x^{\mathrm{IMU}}, d_y^{\mathrm{IMU}}, d_z^{\mathrm{IMU}})$ are the distances between the IMU and the CoG. The variables $(\dot{p}, \dot{q}, \dot{r})$ are derived through numerical differentiation of the rotational

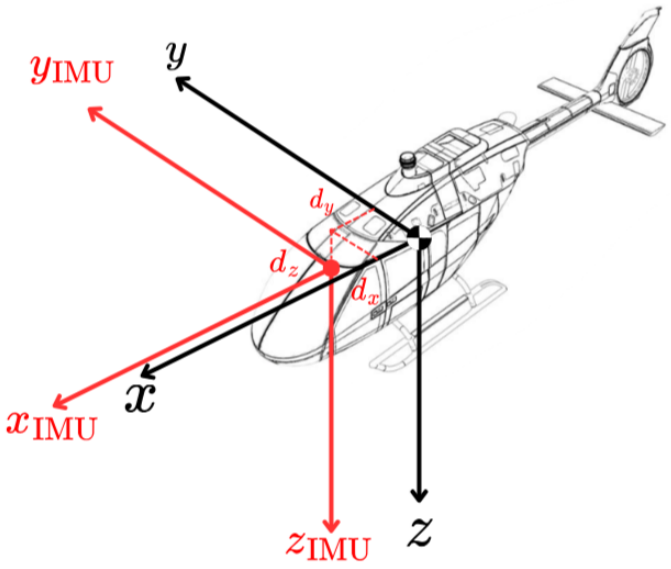


Figure 3.3: Inertial Measurement Unit reference frame

rates $(p, q, r)$. Any sensor misalignment should also be accounted for, however, it is assumed that any offset is negligible, both for the Inertial Measurement Unit and the Air Data Boom. In the first case, it is usually possible to achieve a good level of accuracy during installation while for the ADB, it is virtually impossible to estimate the misalignment as it is highly correlated with sensor bias. Kopter already accounts for a misalignment in the symmetry plane of the helicopter that results in a correction in the Angle of Attack, as shown in figure 3.5. Finally, the flow velocities estimated at the CoG must be computed at the ADB:

$$\begin{cases} u_{\text{ADB}} = u - r d_{y,\text{ADB}} + q d_{z,\text{ADB}} \\ v_{\text{ADB}} = v - p d_{z,\text{ADB}} + r d_{x,\text{ADB}} \\ w_{\text{ADB}} = w - q d_{x,\text{ADB}} + p \cdot d_{y,\text{ADB}} \end{cases} \tag{3.7}$$

where $(d_x^{\text{ADB}}, d_y^{\text{ADB}}, d_z^{\text{ADB}})$ are the distances between the ADB and the CoG. Finally, the measurement equations, comprehensive of the error models, are as follows:

$$V_{\text{m}} = \sqrt{u^2 + v^2 + w^2} \tag{3.8}$$

$$\alpha_{\text{m,ADB}} = K_\alpha \arctan\left(\frac{w_{\text{ADB}}}{u_{\text{ADB}}}\right) + b_\alpha \tag{3.9}$$

$$\beta_{\text{m,ADB}} = K_\beta \arcsin\left(\frac{v_{\text{ADB}}}{\sqrt{u_{\text{ADB}}^2 + v_{\text{ADB}}^2 + w_{\text{ADB}}^2}}\right) + b_\beta \tag{3.10}$$

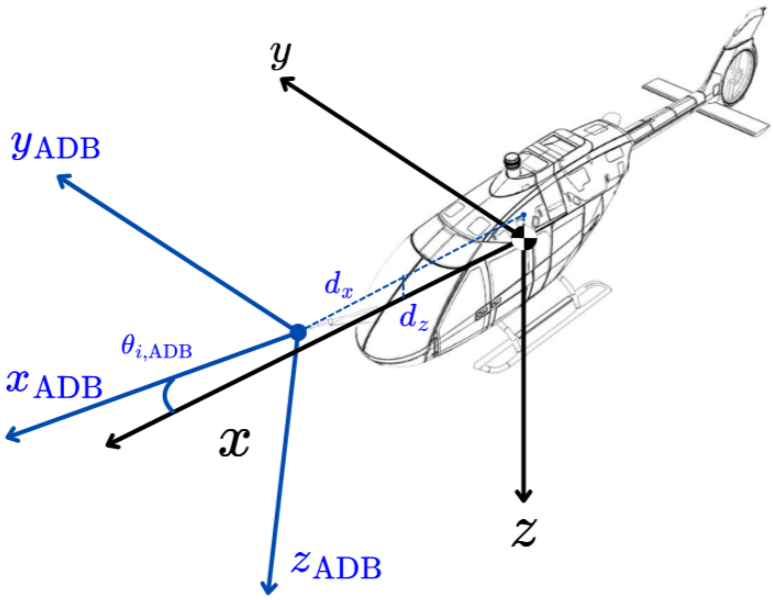


Figure 3.4: Air Data Boom reference frame

In conclusion, FPR aims to find the parameters of the error models, the problem is analogous to parameter estimation and can be solved either with a deterministic or a stochastic approach, depending on the assumptions made. If the noise in the input variables is considered negligible, which is the case for accelerometers and gyros used in this case, a deterministic approach can be used and the states are estimated through numerical integration of the kinematic equations. The error models' parameters are instead estimated through the Output Error Method by incorporating them into the state-space model:

$$\begin{cases} \dot{x} = f(x(t), u(t)|\Theta) & x(t_0) = x_0 \\ y = g(x(t)|\Theta) \end{cases} \tag{3.11}$$

where:

- $x = [u, v, w, \phi, \theta, \psi, h]^{\mathrm{T}}$ is the state vector;
- $u = [a_x, a_y, a_z, p, q, r]^{\mathrm{T}}$ is the input vector;
- $y = [V, \alpha, \beta, \phi, \theta, \psi, h]^{\mathrm{T}}$ is the output vector;
- $\Theta = [b_\alpha, b_\beta, b_{\bar{q}}, K_\alpha, K_\beta, K_{\bar{q}}]^{\mathrm{T}}$ are the unknown parameters to be estimated.

When the noise in the input variables is not negligible a stochastic approach is preferred involving the Extended Kalman Filter (EKF).

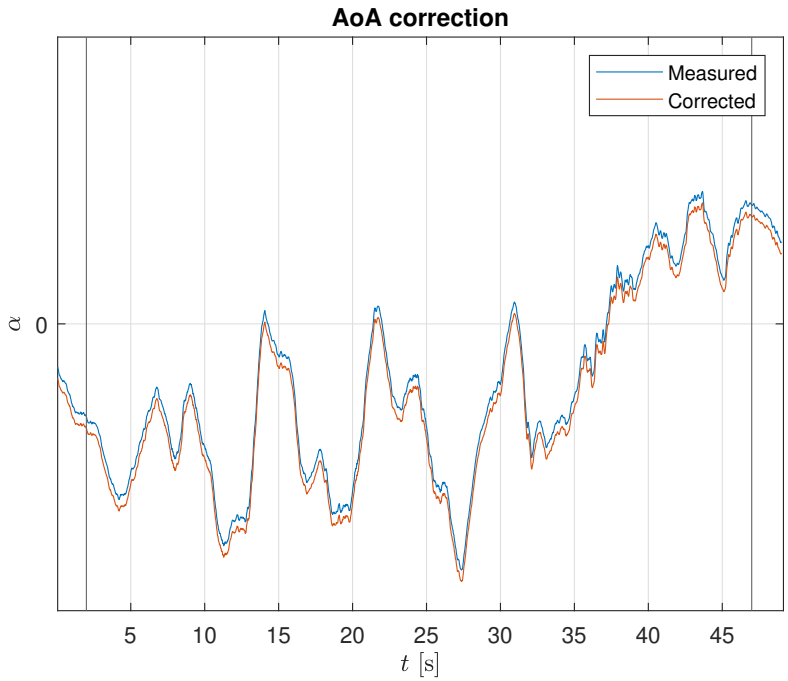


Figure 3.5: Angle of Attack correction

## 3.3 Output Error Method

The Output Error Method (OEM) is widely used in aircraft parameter estimation and thus, in Flight Path Reconstruction. The model's parameters are computed iteratively to minimise the error between the real measurements and the estimated outputs (figure 3.6). An optimisation algorithm updates the parameters at every step, meaning that the process has a high computational cost [2] [5].

### 3.3.1 Maximum likelihood principle

Among the algorithms that aim to solve the optimisation problem posed by the OEM, the maximum likelihood principle makes use of probability theory by defining a likelihood function:

$$p(z|\Theta) = \prod_{k=1}^{N} p(z_k|\Theta) \tag{3.12}$$

where $z_k$ is a vector containing the set of measurements made at timestamp $t_k$, $\Theta$ is the parameter vector and $p(z|\Theta)$ is the probability of obtaining $z$ given $\Theta$. The maximum likelihood method aims to find the vector $\hat{\Theta}_{\text{ML}}$ that maximises $p(z|\Theta)$.

Most probability density functions are exponential so the logarithm of the

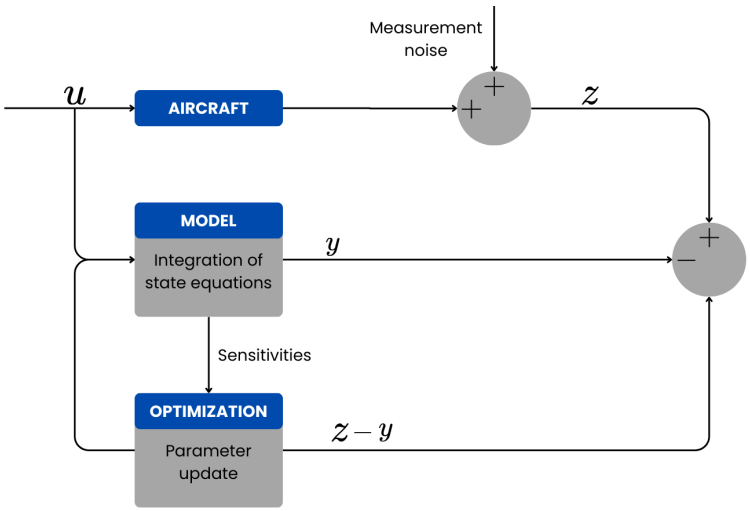


Figure 3.6: Output Error Method scheme, based on [2]

likelihood function can be exploited to achieve the same solution:

$$\hat{\Theta}_{\mathrm{ML}} = \arg\left\{\min_{\Theta}\left[\ln p(z|\Theta)\right]\right\} \tag{3.13}$$

To find $\hat{\Theta}_{\mathrm{ML}}$, the gradient of the logarithm must be zero, so a set of nonlinear equations is obtained:

$$\frac{\partial \ln p(z|\Theta)}{\partial \Theta} = 0 \tag{3.14}$$

Depending on the assumptions on $p(z|\Theta)$, a cost function $J$ is obtained by expanding the left term of 3.14. If a Gaussian density probability is assumed, it can be written as:

$$J(\Theta|R) = \frac{1}{2}\sum_{k=1}^{N}\left[z(t_k) - y(t_k)\right]^T R^{-1}\left[z(t_k) - y(t_k)\right] + \frac{N}{2}\ln\left[\det\left(R\right)\right] + \frac{Nn_y}{2}\ln\left(2\pi\right) \tag{3.15}$$

where:

- $z(t_k)$ is the measurement at time $t_k$;
- $y(t_k)$ is the estimated output at time $t_k$;
- $R$ is the covariance matrix;

- $N$ is the number of observations;
- $n_y$ is the dimension of the measurement vector.

The value of $\Theta$ that gives the highest probability of obtaining the measurements $z$ is the one that minimises the cost function $J$ [2].

One method used to solve these nonlinear problems is the Gauss-Newton algorithm. After having obtained an expression for the cost function, equation 3.14 can be written as:

$$\frac{\partial J(\Theta)}{\partial \Theta} = 0 \tag{3.16}$$

Expanding now the left term through Taylor approximation:

$$\left(\frac{\partial J(\Theta)}{\partial \Theta}\right)_{i+1} \approx \left(\frac{\partial J(\Theta)}{\partial \Theta}\right)_i + \left(\frac{\partial^2 J(\Theta)}{\partial \Theta^2}\right)_i \Delta\Theta \tag{3.17}$$

where $\Delta\Theta$ is the parameter change vector, given by:

$$\Delta\Theta = -\left[\left(\frac{\partial^2 J(\Theta)}{\partial \Theta^2}\right)_i\right]^{-1} \left(\frac{\partial J(\Theta)}{\partial \Theta}\right)_i \tag{3.18}$$

The problem is now linear and can be written as:

$$\Theta_{i+1} = \Theta_i + \Delta\Theta \qquad F\Delta\Theta = -G \tag{3.19}$$

where $F$ is the Hessian or information matrix and $G$ is the gradient vector.

### 3.3.2 Fitlab

During this thesis, Flight Path Reconstruction was implemented through Fitlab, a MATLAB tool developed by the German Aerospace Research Centre DLR (Deutsches Zentrum für Luft- und Raumfahrt).

Fitlab takes as input:

- aerodynamic measurements;
- inertial measurements, such as linear accelerations and rotational rates;
- the set of kinematic equations of motion of the aircraft;
- the vector parameter to be estimated

The vector parameter is initialised setting the biases to 0 and the scale factors to 1 while the states are initialised from the measurements. The state equations are then numerically integrated and the aerodynamic measurements are estimated, the Gauss-Newton method is used to compute the parameter change vector $\Delta\Theta$ to reduce the error between measurements and the reconstructed aerodynamic variables. The process is repeated until the maximum number of iterations is reached or until the relative change of the cost function is below a certain threshold.

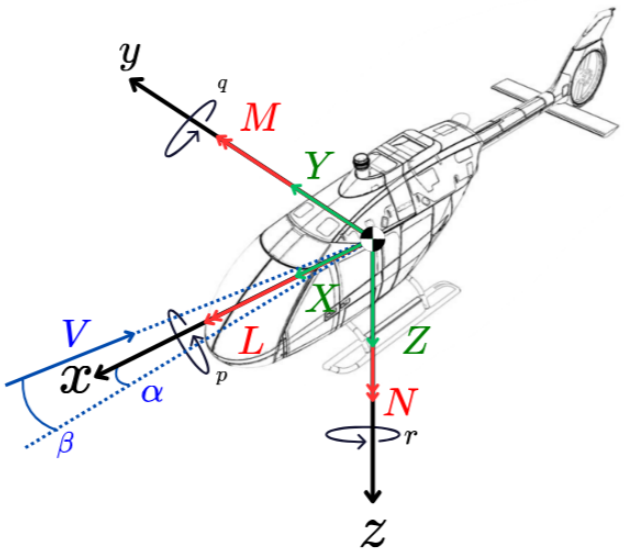


Figure 3.7: Sign conventions

## 3.4 Conventions

This thesis follows the same conventions as the WHeSI project, which are consistent with standard helicopter flight mechanics [6]. Figure 3.7 shows the reference frames used and the resulting sign conventions.

As per the control inputs, the *AW09* has a clockwise rotating main rotor, so a positive pedal input $\eta_p$ must create a clockwise yawing moment to counteract the counterclockwise torque of the main rotor. The remaining controls have standard sign conventions, positive collective increases the pitch of the blades and results in a gain of altitude, positive longitudinal cyclic pitches the aircraft forward while positive lateral cyclic induces a right-hand roll.

# Chapter 4

# Data processing

In the first half of 2024, Kopter conducted a test campaign around Mollis Airport with HB-ZXD. During each flight, the telemetry was transmitted in real-time to the ground station where it was stored in TDMS files. A test log was also manually updated with the tasks performed by the helicopter.

As the test campaign was not conducted for system identification purposes, only some tests contained useful data for Flight Path Reconstruction. After reviewing the test logs, 12 flights were selected based on the manoeuvres performed in each.

Once the data was received, several tasks were carried out to prepare it for Flight Path Reconstruction. The FPR framework is coded entirely on MATLAB so the files were first converted to MATLAB timetables and then broken down into short segments each containing a single manoeuvre.

## 4.1 Conversion from TDMS to MATLAB timetable

### 4.1.1 TDMS files

Technical Data Management Streaming (TDMS) is a file format developed by National Instruments (NI) that allows for consistent and organised data storage [12].

TDMS files are hierarchically organised into three levels, at the top there is an object that holds information about the file, like the title or the author. The data is then categorised into groups (second level) and each signal is stored in a channel (third level). A path can be used to access the signals, it consists of a unique string that contains the names of the group and the channel. Each level has several objects that can store useful information, such as the sample rate, the number of samples or the data format.

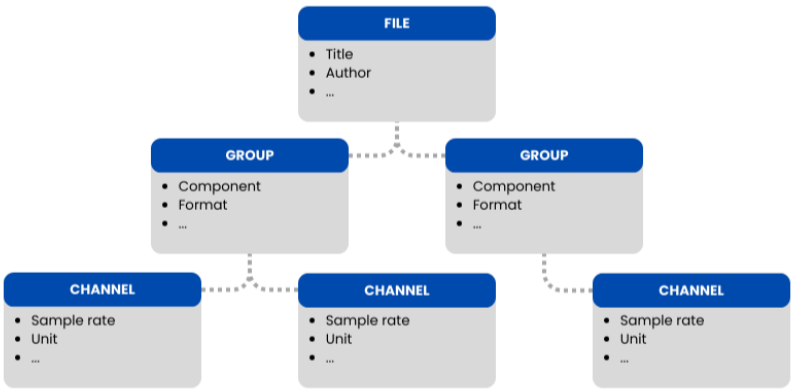


Figure 4.1: TDMS file internal structure

Using DIAdem (NI software), the TDMS files were analysed to determine how the signals were grouped and which signals were useful to the purpose of this thesis. By discarding the unwanted signals it was possible to reduce significantly the size of the files and the time needed for conversion. Only the channels whose names contained these keywords were kept:

- *'ADAHRS'*, *'ESIS'* and *'GIA'* for inertial measurements coming respectively from the Air Data Attitude Heading Reference System, Electronic Standby Instrument System and the Garmin G3000 instruments;
- *'NB'* for aerodynamic measurements recorded by the Nose Boom;
- *'HC'* for weight and balance parameters;
- *'CNT'* for control inputs measured as collective, cyclic and pedal deflections.

Note that the signals coming from the ESIS and the Garmin G3000 were selected only as references for the ADAHRS as a means of preliminary data compatibility check [5] but were not used for FPR purposes.

Two files were available for each test flight, one labelled as 'raw' and the other as 'processed'. In the latter, the signals were upsampled and some corrections were applied, introducing time delays that could impact subsequent analysis, on the other hand, some of the selected channels were present exclusively in this file. Because of the possible corruption of the 'processed' data, it was decided to use the 'raw' file whenever possible and extract only the missing signals from the 'processed' file.

Tables A.1.1 to A.1.6 show the extracted signals and their parameters.

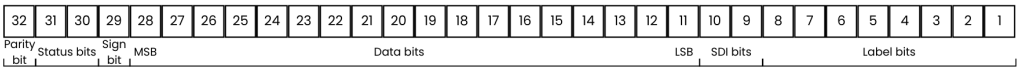


Figure 4.2: ARINC 429 binary (BNR) data structure

### 4.1.2 ARINC decoding

Special attention was given to some signals coming from the ESIS and the Garmin instruments, labelled as *'ESIS/GIA1/2_ARI_LABEL_XXX_RAW'*, where XXX is a three-digit label. As the name suggests, these signals were encoded through the ARINC 429 protocol and had to be decoded prior to use. All useful signals were binary coded (BNR) in a 32-bit sequence (figure 4.2) with the following format [7]:

- bits 1 to 8 when converted to the octal base yield the three-digit label of the signal;
- bits 9 and 10 are the source/destination identifiers (SDI) bits;
- bits 11 to 28 contain the data;
- bit 29 is the sign bit;
- bits 30 and 31 are the status bits;
- bit 32 is a parity bit to detect any error.

The latter is the most significant bit so the sequence must be flipped before decoding.

The encoded data is stored in $N$ significant bits (with $N$ varying among different signals) and must be converted from binary to decimal base. Once a decimal number is obtained, it must be multiplied by the value of the least significant bit $v_{\text{LSB}}$, also called the resolution of the signal. This value depends on the range of values $R$ that the signal may adopt and the number of significant bits $N$ according to the following relationship:

$$v_{\text{LSB}} = \frac{R}{2^N} \tag{4.1}$$

A brief example of the decoding process will now be presented for one timestamp of the channel *'GIA2_ARI_LABEL_325_RAW'*:

```
1 00 1 11111001110000000 00 10101011
```

first, the label must be verified, flipping the last 8 digits and converting to octal base:

$$\texttt{10101011} \Rightarrow 11010101_2 \Rightarrow 325_8 \tag{4.2}$$

which is correct and according to the label-to-signal table in [7], 325 is the label assigned to the roll angle $\phi$. Moving on to the data sequence, again the bits must be flipped and converted to the decimal base:

$$\texttt{11111001110000000} \Rightarrow 00000011100111111_2 \Rightarrow 1855_{10} \tag{4.3}$$

this value must be scaled to account for range ($R = 180°$ for roll angle) and significant bits ($N = 14$):

$$|\phi| = 1855 \cdot \frac{180°}{2^{14}} = 20.38° \tag{4.4}$$

The sign bit is `1` (negative) so the roll angle at the instant of measuring is $\phi = -20.38°$.

### 4.1.3 Conversion to MATLAB timetable

Once all the signals were in a consistent format, the script `TDMStoMAT.m` was executed to create a single MATLAB timetable containing all channels. The first step of the process aimed to sync the various signals as start and end times varied slightly among channels and each piece of equipment has a different sample rate. A master time vector was then created, starting at the latest start time and ending at the earliest finish time, rounded respectively up and down to the nearest second. The sample rate was set to 100 Hz (the same as the ADAHRS signals) and each signal was linearly interpolated and added to the master timetable.

After the conversion process, it was possible to perform a preliminary data compatibility check through visual inspection. As stated in chapter 3, this is a quick and easy way to spot any major discrepancy, like different sign conventions or units of measurement. The ESIS and Garmin instrumentation measurements were of particular use as they were used for comparison, figure 4.3 shows the attitude measurements for the three channels.

## 4.2 Flight test data slicing

As it will be clear in chapter 5, dividing each flight into single manoeuvres is necessary to perform FPR. This process was performed by manually comparing the flight logs to the plots of the extracted signals. The start and end timestamps of each manoeuvre were then stored in an Excel datasheet (`Manoeuvre_Cut.xslx`),

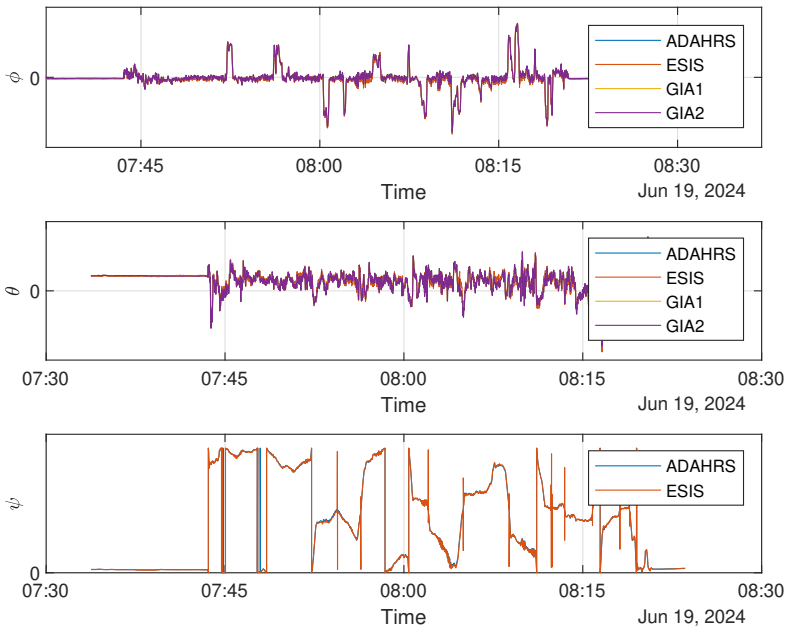


Figure 4.3: Attitude measurements of ADAHRS, ESIS and GARMIN instruments

as well as the name of the manoeuvre and the speed and altitude at the beginning of the flight segment. This task was performed for each flight obtaining a total of 196 manoeuvres, a summary of which can be seen in table 4.1.

A MATLAB function (`cutToManoeuvres.m`) was then used to break down the data from an entire flight test into single segments following the timestamps listed in the spreadsheet `Manoeuvre_Cut.xslx`. A 2-second offset was applied both to the start and end of the segment for better visualisation, this parts were however not included in the FPR process.

Each manoeuvre was stored in a file, named to include several information, such as the flight test number, an incremental manoeuvre ID, the name of the manoeuvre and the initial speed and altitude. This allowed to filter effectively the manoeuvres later on in the FPR process. For example, `FID_107.MID_0025.Alt_4000.S_110.Mnvr_BtB.m` is a MATLAB timetable of a bank-to-bank manoeuvre performed during flight 107 at 4000 ft and 110 kt, this is the 25th identified manoeuvre of the flight.

After analysing the data, the following manoeuvres were identified:

- Bank-to-bank rolls usually from $30°/45°$ to $-30°/-45°$;
- Collective and cyclic frequency sweeps;
- Lateral directional modes oscillations;

| Manoeuvre | Keyword | Amount | Cumulative time |
|---|---|---|---|
| Bank-to-bank | BtB | 9 | 00:09:57 |
| Collective sweeps | ColSw | 2 | 00:00:56 |
| Lateral cyclic sweeps | LatSw | 2 | 00:00:57 |
| Lateral-directional oscillations | LDO | 51 | 00:29:35 |
| Longitudinal cyclic sweeps | LngSw | 2 | 00:01:13 |
| Steady Heading Steady Sideslip | SHSS | 46 | 00:20:55 |
| Turn | Trn | 68 | 00:54:09 |
| Turn on one control (cyclic) | To1cCy | 8 | 00:06:56 |
| Turn on one control (pedal) | To1cPd | 8 | 00:04:28 |
| Total | | 196 | 02:09:06 |

Table 4.1: Summary of identified manoeuvres

- Steady heading steady sideslip flight;
- Turns, including steady-state, windup and on one control (pedal or lateral cyclic).

Figure 4.4 shows the plots of various signals from a lateral cyclic frequency sweep manoeuvre.

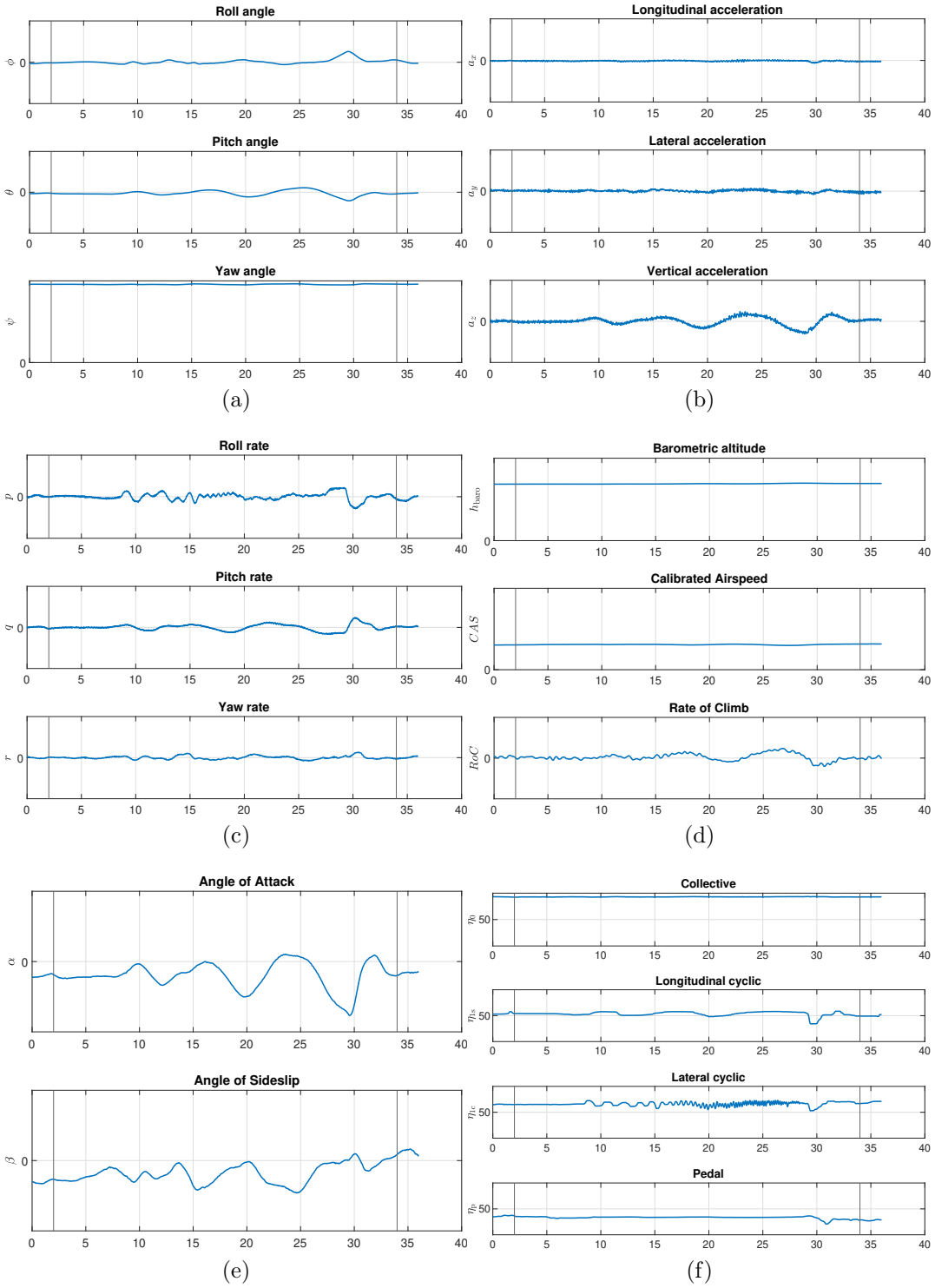


Figure 4.4: Manoeuvre example (frequency sweep)

# Chapter 5

# Flight Path Reconstruction

## 5.1 FPR workflow

The Flight Path Reconstruction process is iterative and consequently requires much time and computational power. The error model parameter estimation is performed for one type of manoeuvre at a time, at each step, the new values are estimated starting from the results obtained for the previous manoeuvre. If the parameters change significantly, the process must be restarted until an adequate fit of all manoeuvres is reached. The chosen sequence is shown in figure 5.1. First, climb segments and Steady Heading Steady Sideslip manoeuvres are reconstructed to explore a good range of AoA and AoS. Subsequently, manoeuvres with a higher dynamic content are analysed: lateral-directional oscillations, turns on one control and control input frequency sweeps. For each manoeuvre, one error model is estimated at a time, first for $\alpha$, then $\beta$ and finally $TAS$. After several tries, it was deemed necessary also to implement an error model for the accelerometer to match the measurements better.

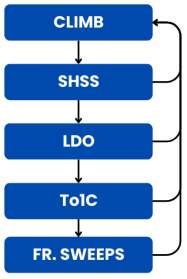


Figure 5.1: Manouevres sequence

## 5.2 Error models

### 5.2.1 AoA correction

The angle of attack error model is straightforward, it is supposed that the AoA sensor has a bias $b$ and a scale factor $K$:

$$\alpha_{\mathrm{m}} = K_\alpha \alpha_{\mathrm{c}} + b_\alpha \implies \alpha_{\mathrm{c}} = \frac{\alpha_{\mathrm{m}} - b_\alpha}{K_\alpha} \tag{5.1}$$

### 5.2.2 AoS correction

The error model for the angle of sideslip is analogue to the one of the AoA:

$$\beta_{\mathrm{m}} = K_\beta \beta_{\mathrm{c}} + b_\beta \implies \beta_{\mathrm{c}} = \frac{\alpha_{\mathrm{m}} - b_\alpha}{K_\alpha} \tag{5.2}$$

### 5.2.3 TAS correction

On aircraft, true airspeed is not measured directly but computed from pressure measurements. The error model is therefore applied to the dynamic pressure, once the measurement is corrected, the true airspeed can be computed from the corrected Mach number:

$$M_{\mathrm{c}} = \sqrt{\frac{2}{\gamma - 1}\left[\left(\frac{\bar{q}_{\mathrm{c}}}{p_{\mathrm{s}}}\right) + 1\right]^{\frac{\gamma-1}{\gamma}} - 1} \implies TAS_{\mathrm{c}} = \frac{M_{\mathrm{c}}}{c} \tag{5.3}$$

Once the dynamic pressure measurement is corrected, the true airspeed can be computed from the corrected Mach number:

$$\bar{q}_{\mathrm{m}} = K_{\bar{q}} \bar{q}_{\mathrm{c}} + b_{\bar{q}} \implies \bar{q}_{\mathrm{c}} = \frac{\bar{q}_{\mathrm{m}} - b_{\bar{q}}}{K_{\bar{q}}} \tag{5.4}$$

### 5.2.4 Linear accelerations measurement

The error model of the accelerometer only includes biases:

$$\begin{cases} a_{x,\mathrm{m}} = a_{x,\mathrm{c}} + b_{a_{x,\mathrm{m}}} \implies a_{x,\mathrm{c}} = a_{x,\mathrm{m}} - b_{a_{x,\mathrm{m}}} \\ a_{y,\mathrm{m}} = a_{y,\mathrm{c}} + b_{a_{y,\mathrm{m}}} \implies a_{y,\mathrm{c}} = a_{y,\mathrm{m}} - b_{a_{y,\mathrm{m}}} \\ a_{z,\mathrm{m}} = a_{z,\mathrm{c}} + b_{a_{z,\mathrm{m}}} \implies a_{z,\mathrm{c}} = a_{z,\mathrm{m}} - b_{a_{z,\mathrm{m}}} \end{cases} \tag{5.5}$$

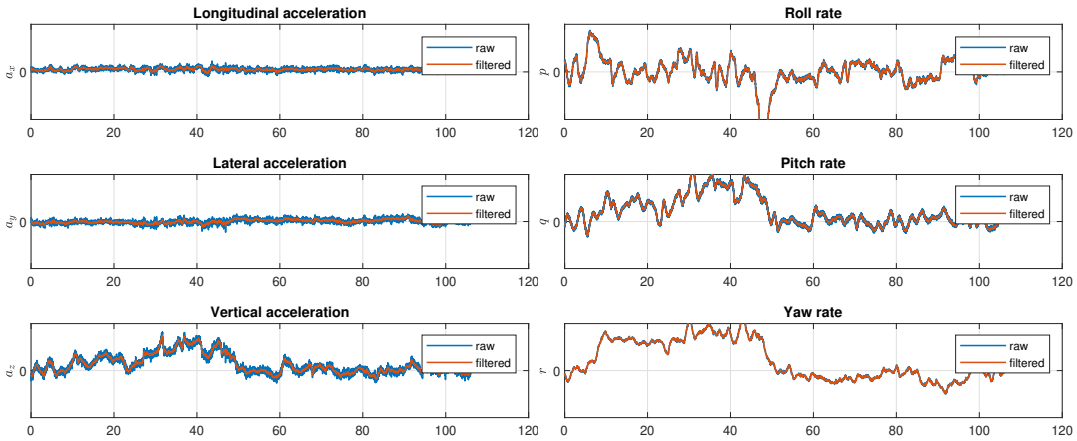


(a) Linear accelerations (b) Rotational rates

Figure 5.2: Filter effect on IMU measurements

## 5.3 FPR process

As already stated in chapter 3 the parameter estimation was carried out through Fitlab, a MATLAB tool developed by the DLR for aircraft parameter estimation.

The input vector contains the linear accelerations and rotational rates, both measured by the IMU inside the ADAHRS unit.

$$u = [a_x, a_y, a_z, p, q, r] \tag{5.6}$$

These variables were preventively filtered through a low pass filter to reduce high-frequency noise that could invalidate the numerical integration, figure 5.2 shows the filter's effect.

The output vector contains the aerodynamic variables, the Euler angles and the altitude:

$$y = [TAS, \alpha, \beta, \phi, \theta, \psi, h] \tag{5.7}$$

The parameters of the error models are in the vector $\Theta$:

$$\Theta = \left[b_\alpha, K_\alpha, b_\beta, K_\beta, b_{\bar{q}}, K_{\bar{q}}, b_{a_x}, b_{a_y}, b_{a_z}\right] \tag{5.8}$$

First, the aircraft kinematic equations are initialised from aerodynamic measurements. True Air Speed, AoA and AoS are corrected by applying the inverse

formula of 5.1, 5.2 and 5.4:

$$\begin{gathered}\alpha_c = \frac{\alpha_m - b_\alpha}{K_\alpha} \\ \beta_c = \frac{\beta_m - b_\beta}{K_\beta} \\ \bar{q}_c = \frac{\bar{q}_m - b_{\bar{q}}}{K_{\bar{q}}} \implies M_c = \sqrt{\frac{2}{\gamma - 1}\left[\left(\frac{\bar{q}_c}{p_s}\right) + 1\right]^{\frac{\gamma-1}{\gamma}} - 1} \implies \\ TAS_c = \frac{M_c}{c}\end{gathered} \tag{5.9}$$

Flow velocities at the Air Data Boom are then computed through simple trigonometric relations:

$$\begin{cases} u_{\text{ADB}} = TAS_c \cos\alpha_c \cos\beta_c \\ v_{\text{ADB}} = TAS_c \sin\beta_c \\ w_{\text{ADB}} = u \tan\alpha_c \end{cases} \tag{5.10}$$

To initialise the state vector, the flow velocities must be computed at the centre of gravity. The inverse formula of equation 3.7 must be applied:

$$\begin{cases} u_{\text{CoG}} = u_{\text{ADB}} + r \cdot d_{y,\text{ADB}} - q \cdot d_{z,\text{ADB}} \\ v_{\text{CoG}} = v_{\text{ADB}} + p \cdot d_{z,\text{ADB}} - r \cdot d_{x,\text{ADB}} \\ w_{\text{CoG}} = w_{\text{ADB}} + q \cdot d_{x,\text{ADB}} - p \cdot d_{y,\text{ADB}} \end{cases} \tag{5.11}$$

The altitude is also initialised from the static pressure measurement, meanwhile the Euler angles are initialised from ADAHRS measurements. For each measurement, the mean of the first 5 samples of each variable is computed to obtain the initial condition vector.

$$x_0 = [u_{0,\text{CoG}}, v_{0,\text{CoG}}, w_{0,\text{CoG}}, \phi_0, \theta_0, \psi_0, h_0] \tag{5.12}$$

Once the state vector is initialised, linear accelerations are corrected for their biases and the kinematic equations of motion (equation 3.2) are integrated through the forward Euler numeric method, obtaining the state vector estimation for the duration of the selected manoeuvre. The estimated velocities need to be computed at the ADB:

$$\begin{cases} u_{\text{ADB}} = u_{\text{CoG}} - r \cdot d_{y,\text{ADB}} + q \cdot d_{z,\text{ADB}} \\ v_{\text{ADB}} = v_{\text{CoG}} - p \cdot d_{z,\text{ADB}} + r \cdot d_{x,\text{ADB}} \\ w_{\text{ADB}} = w_{\text{CoG}} - q \cdot d_{x,\text{ADB}} + p \cdot d_{y,\text{ADB}} \end{cases} \tag{5.13}$$

The aerodynamic variables are then obtained from trigonometric relations:

$$\begin{cases} TAS = \sqrt{u_{\text{ADB}}^2 + v_{\text{ADB}}^2 + w_{\text{ADB}}^2} \\ \alpha = \arctan \frac{w_{\text{ADB}}}{u_{\text{ADB}}} \\ \beta = \arcsin \frac{v_{\text{ADB}}}{TAS} \end{cases} \tag{5.14}$$

To compare the measured and estimated aerodynamic variables, the error model must be applied again:

$$\begin{gathered} \alpha_{\text{r}} = K_\alpha \alpha + b_\alpha \\ \beta_{\text{r}} = K_\beta \beta + b_\beta \\ M = \frac{TAS}{c} \implies \bar{q} = p_{\text{s}} \left[ \left( 1 + \frac{\gamma - 1}{2} M^2 \right)^{\frac{\gamma}{\gamma - 1}} - 1 \right] \implies \\ \bar{q}_{\text{r}} = K_{\bar{q}} \bar{q} + b_{\bar{q}} \implies M_{\text{r}} = \sqrt{\frac{2}{\gamma - 1} \left[ \left( \frac{\bar{q}_{\text{r}}}{p_{\text{s}}} \right) + 1 \right]^{\frac{\gamma - 1}{\gamma}} - 1} \implies TAS_{\text{r}} = M_{\text{r}} \cdot c \end{gathered} \tag{5.15}$$

Once the reconstructed variables vector is computed, the Output Error Method is applied and an iterative optimization algorithm adjusts the unknown parameters until the error between measurements and reconstructed variables is minimised. The algorithm is stopped when the relative change in cost $J$ is below $1e-06$, the maximum amount of iterations was set to 50, but it was never reached.

## 5.4 Results

### 5.4.1 Error models

The error models' parameters for angle of attack, angle of sideslip, true airspeed and linear accelerations are shown in tables 5.1, 5.2, 5.3 and 5.4.

| Parameter | Value |
|---|---|
| $b_\alpha$ | -1.4316° |
| $K_\alpha$ | 0.913 |

Table 5.1: Angle of Attack error model parameters

Figures 5.3 to 5.6 show the variables' match and their residuals before and after applying the error model for one of each manoeuvre.

| Parameter | Value |
|---|---|
| $b_\beta$ | -4.2417° |
| $K_\beta$ | 0.792 |

Table 5.2: Angle of Sideslip error model parameters

| Parameter | Value |
|---|---|
| $b_{\bar{q}}$ | 236.34 Pa |
| $K_{\bar{q}}$ | 0.615 |

Table 5.3: Dynamic pressure error model parameters

| Parameter | Value |
|---|---|
| $b_{a_x}$ | 0.505 m/s$^2$ |
| $b_{a_y}$ | 0.019 m/s$^2$ |
| $b_{a_z}$ | -0.049 m/s$^2$ |

Table 5.4: Accelerometer error model parameters

### 5.4.2 Climbs

During climbs the helicopter gains altitude while in a trimmed condition. The pitch is maintained constant and the bank angle is almost zero. Figure 5.7 shows the difference between measured and reconstructed variables for five climbs. As expected, the estimated Euler angles match perfectly, while the reconstruction accuracy of the aerodynamic variables varies. Overall, $TAS$ reconstruction is solid, but the same can't be said for AoA and AoS, whose reconstruction presents a drift in almost every manoeuvre. Altitude gain $\Delta h$ is reproduced with adequate fidelity.

### 5.4.3 Steady Heading Steady Sideslips

During a Steady Heading Steady Sideslip manoeuvre the pilot maintains a constant sideslip by pointing the helicopter's nose at an angle to the relative wind. FPR results for this manoeuvres are visible in figure 5.8. The model fails to properly reconstruct the angle of sideslip $\beta$, showing an almost constant drift in one direction or the other, depending on the sign of the AoS. AoA and TAS fits are mostly adequate, with some exceptions. Climbing and descending SHSS manoeuvres are shown in figure 5.9 and 5.10, the same comments can also be applied to

these conditions. In some cases, where the absolute values of $\beta$ are lower, the reconstruction is better. The model also struggles to reproduce altitude loss.

### 5.4.4 Lateral-directional oscillations

LDOs were performed almost exclusively during climbs, the pilot induced the oscillations through a sinusoidal lateral cyclic input to excite the dutch roll mode and evaluate the aircraft's handling capabilities. As can be seen in figure 5.11, the reconstructed angle of sideslip and angle of attack match the measured flow angles for most of the cases but some amplitude damping can be seen for $\beta$. For TAS, the overall trend seems to be reproduced correctly, while high frequency variations are not.

### 5.4.5 Turns on one control

To achieve a coordinated turn, the pilot must input both lateral cyclic and pedal. If this is not the case, a sideslip angle $\beta$ is developed. Flight path reconstruction of turns on one control (figure 5.12) is adequate for AoS while AoA oscillations seem to be amplified. The last manoeuvre is an outlier for every variable, indicating that external conditions may be the reason for the bad match.

### 5.4.6 Control input frequency sweeps

Two sets of cyclic and collective frequency sweeps were performed during the test campaign. In these manoeuvres, the pilot increased the frequency of one input at a time to evaluate the aircraft's response. A plot containing the FPR results is shown in figure 5.13. The angle of sideslip reconstruction is good in some cases, while AoA oscillations are amplified as was the case for the previous manoeuvre. TAS has a constant negative drift, all the frequency sweep manoeuvres were recorded during the same flight, this could indicate that external factors are the cause of the anomalous behaviour.

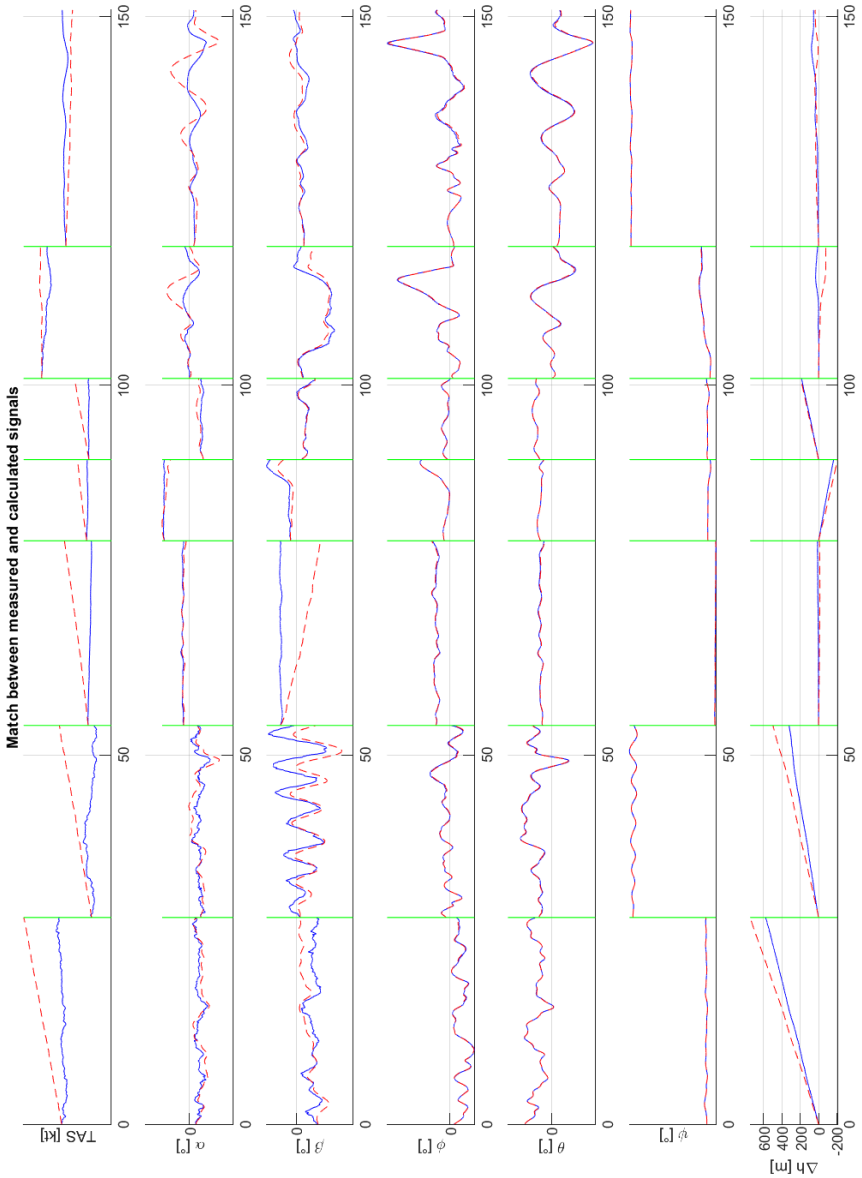


Figure 5.3: Matching plot without error model, blue: measured, red: reconstructed

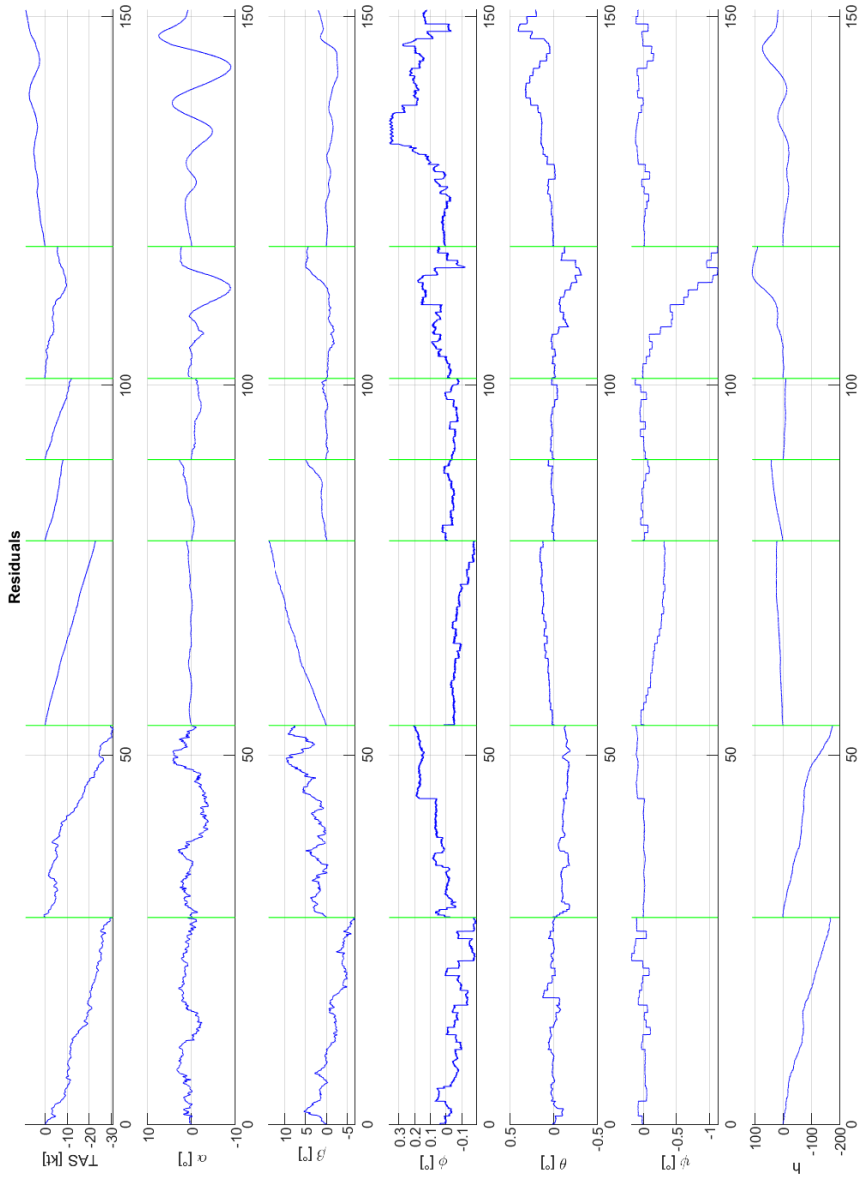


Figure 5.4: Residuals plot without error model

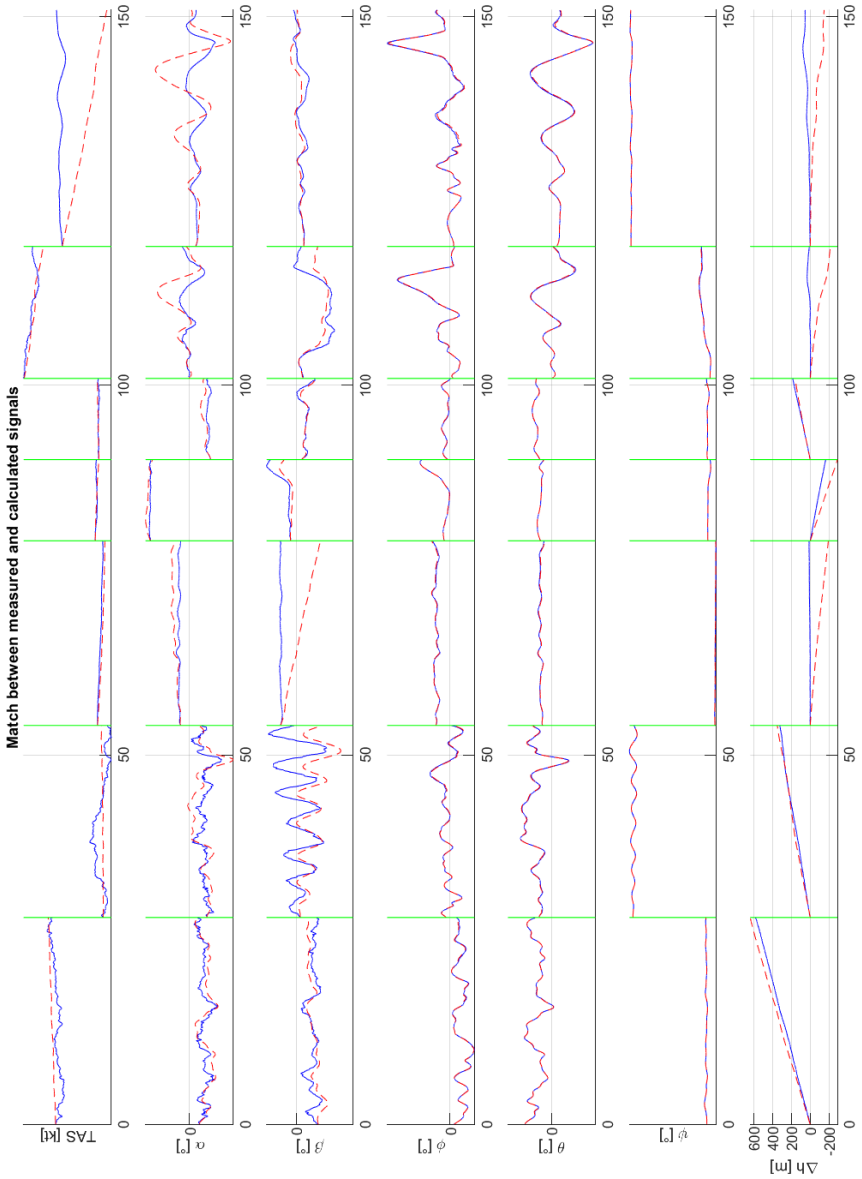


Figure 5.5: Matching plot with error model, blue: meas., red: recon.

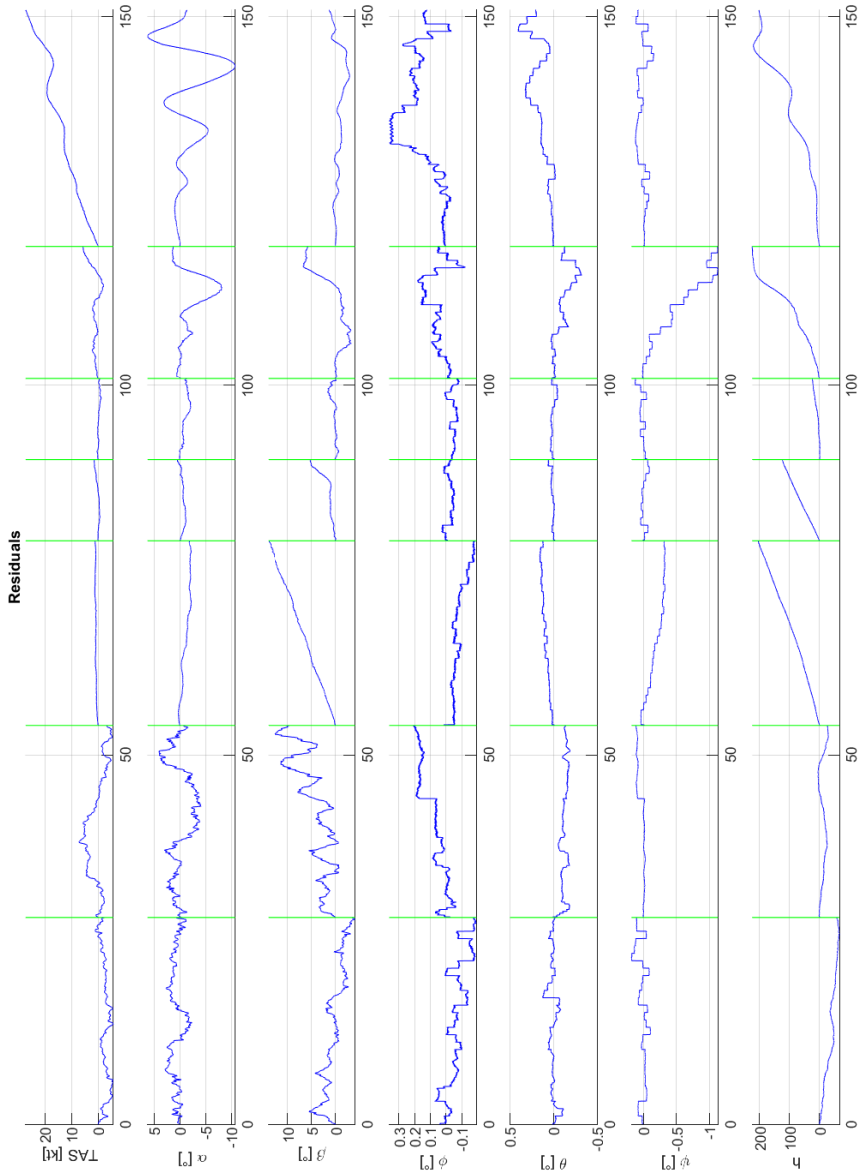


Figure 5.6: Residuals plot with error model

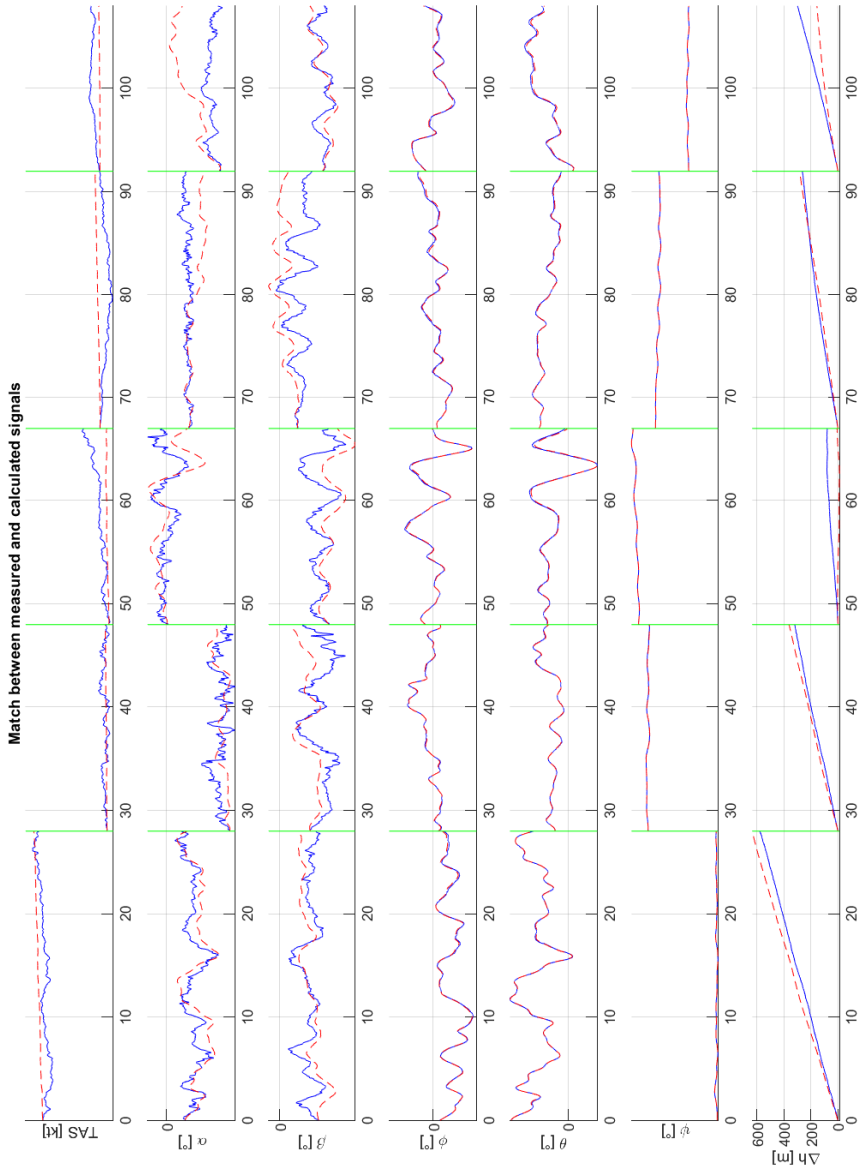


Figure 5.7: Matching plot for climbs, blue: meas., red: recon.

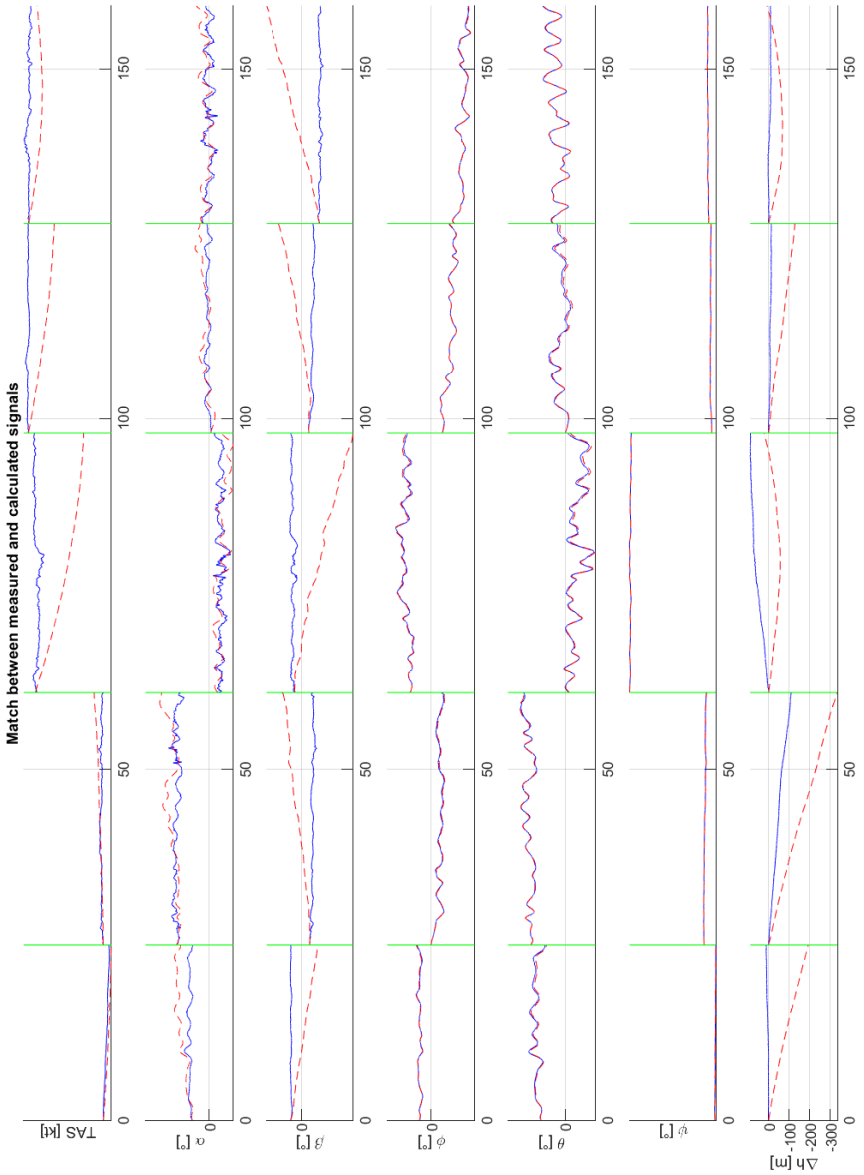


Figure 5.8: Matching plot for SHSS, blue: meas., red: recon.

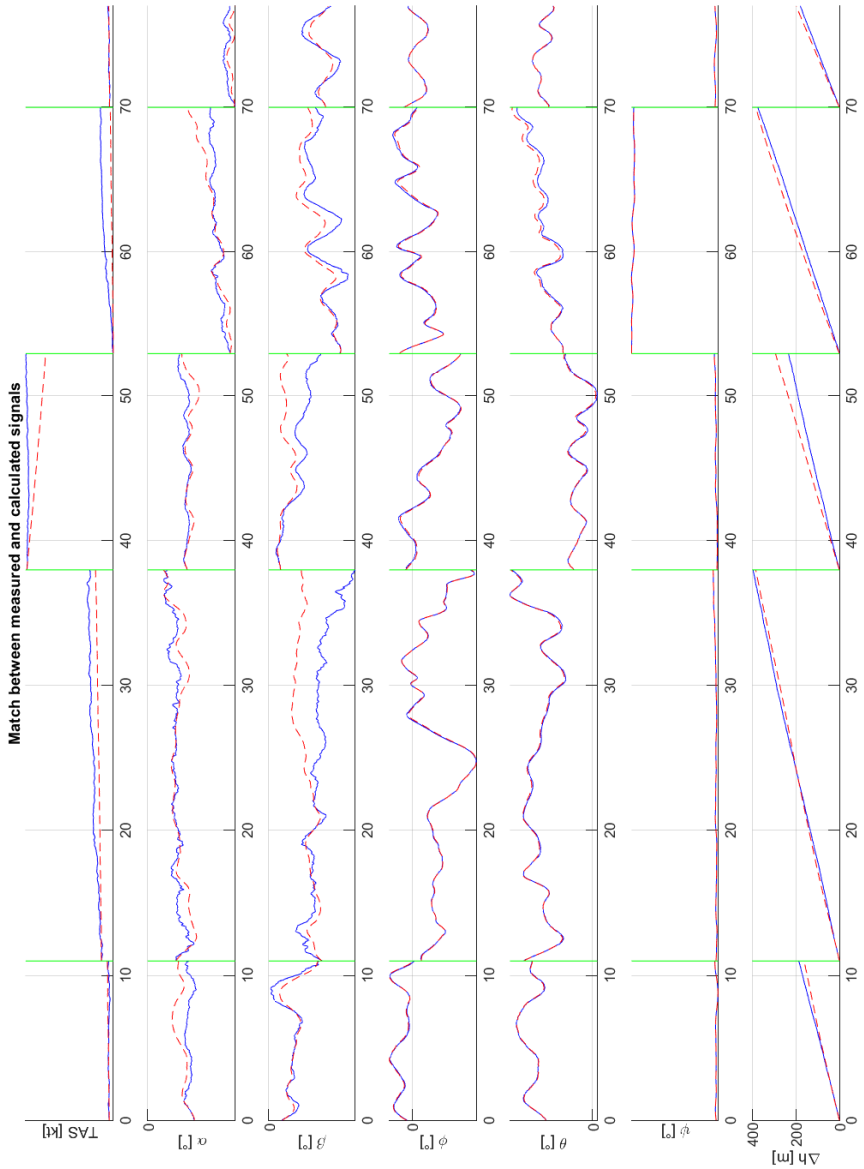


Figure 5.9: Matching plot for climbing SHSS, blue: meas., red: recon.

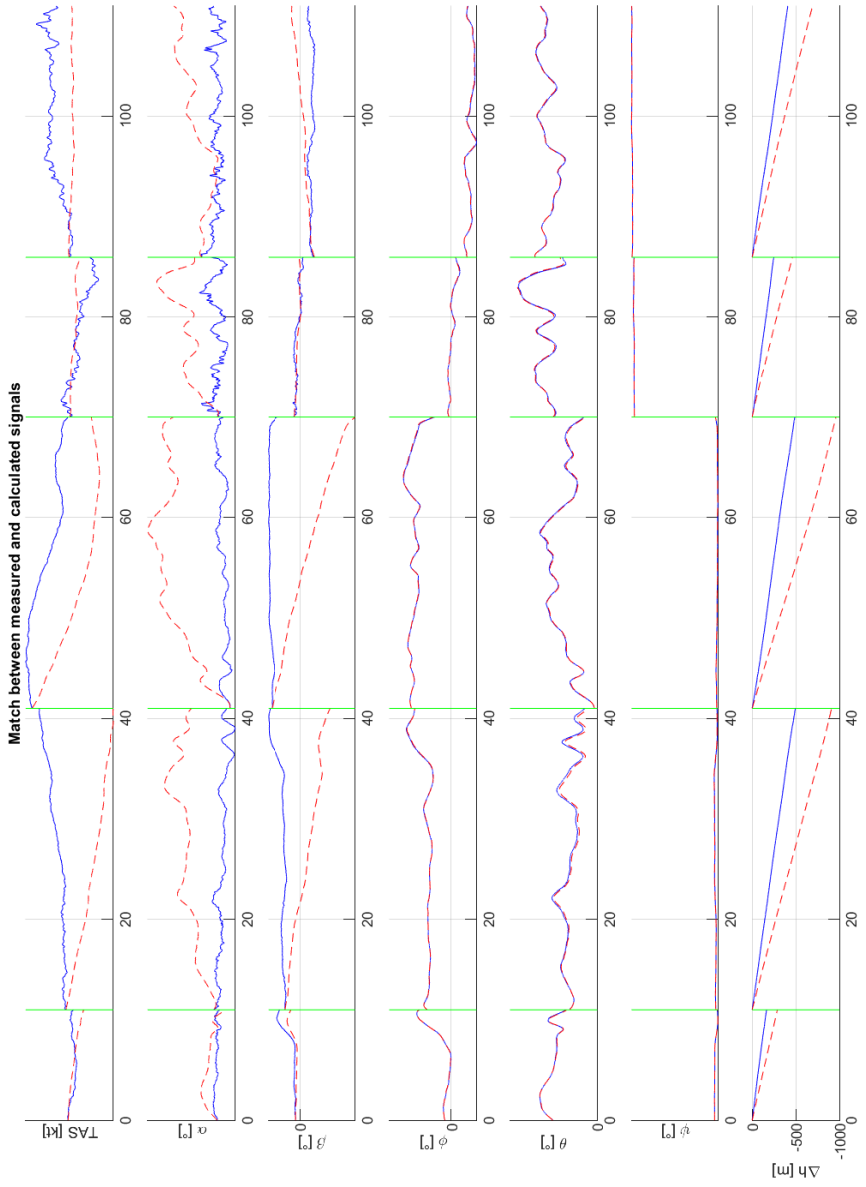


Figure 5.10: Matching plot for descending SHSS, blue: meas., red: recon.

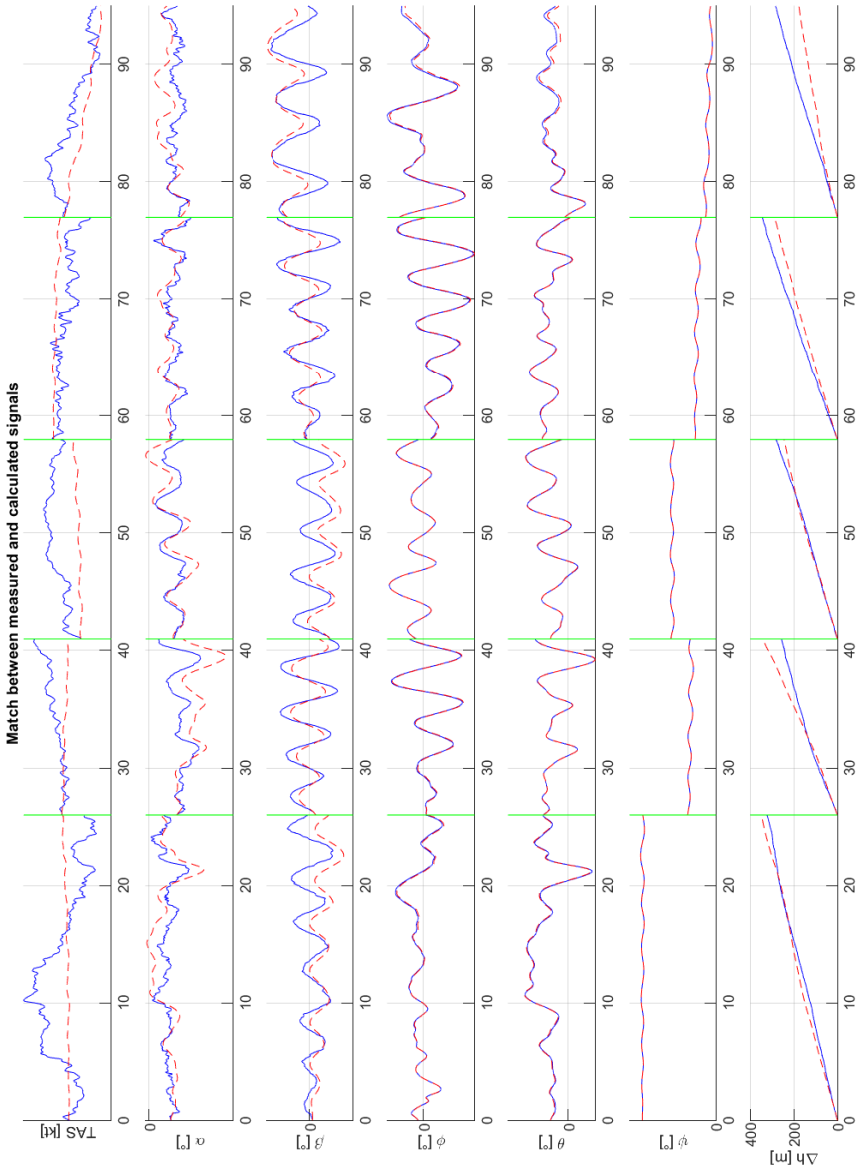


Figure 5.11: Matching plot for LDOs, blue: meas., red: recon.

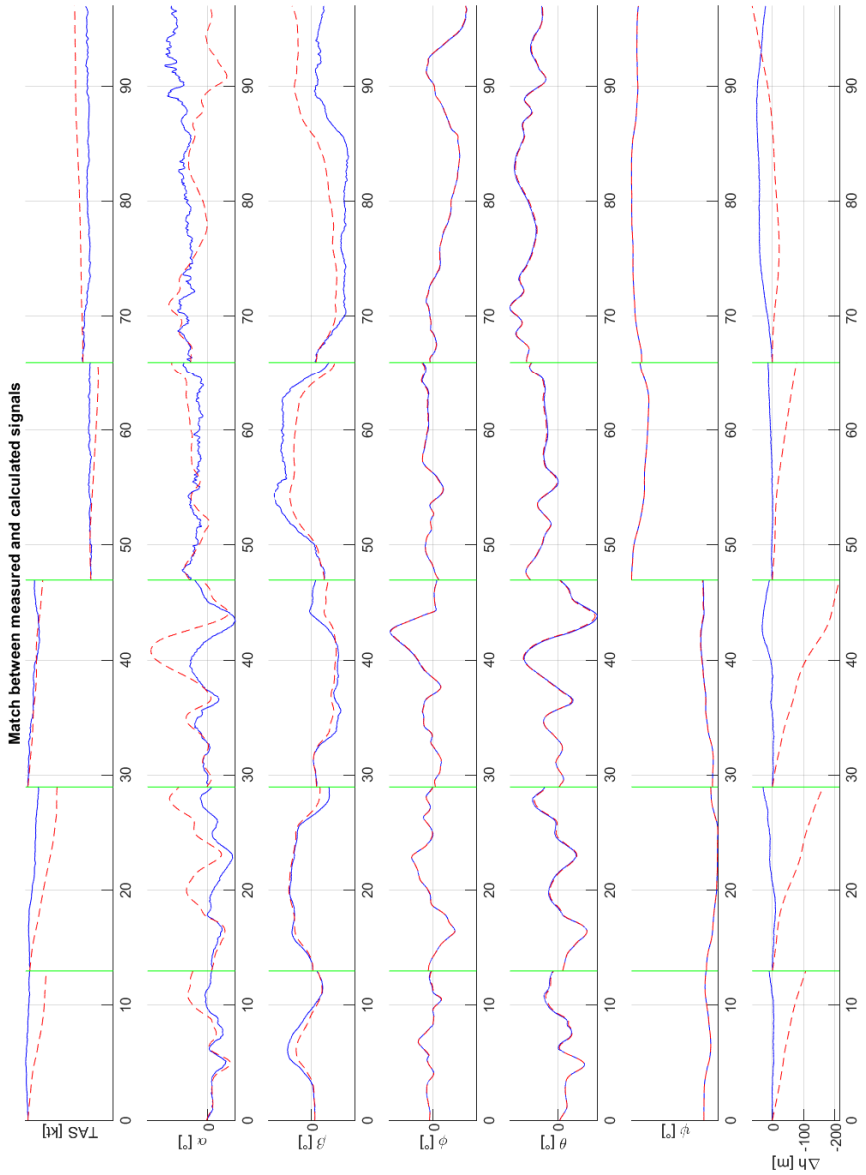


Figure 5.12: Matching plot for To1C, blue: meas., red: recon.

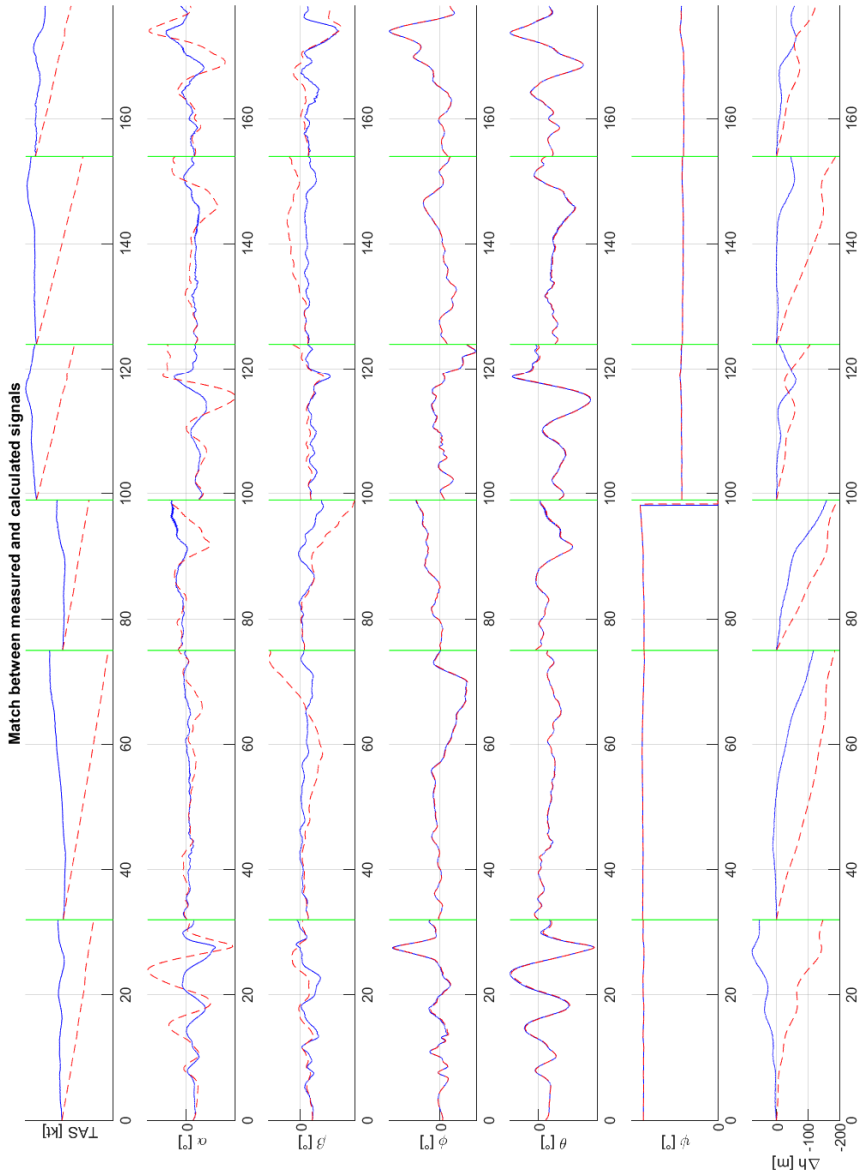


Figure 5.13: Matching plot for frequency sweeps, blue: meas., red: recon.

# Conclusion

As already stated, flight path reconstruction is a crucial step in aircraft test data analysis and system identification. The objective of this thesis was to build a solid base for future FPR activities, not to find a perfect fit, practically impossible nevertheless. Considering that system identification was not the main goal for the test campaign, that the ADAHRS is designed as part of the flight instrumentation, not as a flight test data recording unit, and finally, that the wind is supposed constant, the fit achieved can be considered satisfactory.

Attempts were made to further refine the model by including cross-dependency between the variables, however, they were unsuccessful. Future works regarding FPR on new test data of the *Kopter AW09* will be conducted with more accurate and suited instrumentation that will certainly help to fill the gaps that are left from this work.

# Appendix

## A.1 Signals

| Channel name | Signal | Unit | Sample rate |
|---|---|---|---|
| *'ADAHRS_ARI_ACC_HCX'* | Long. accel. | g | 100 Hz |
| *'ADAHRS_ARI_ACC_HCY'* | Lat. accel. | g | 100 Hz |
| *'ADAHRS_ARI_ACC_HCZ'* | Vert. accel. | g | 100 Hz |
| *'ADAHRS_ARI_ANG_MAGHEAD'* | Heading (magn.) | ° | 50 Hz |
| *'ADAHRS_ARI_ANG_PIT'* | Pitch angle | ° | 100 Hz |
| *'ADAHRS_ARI_ANG_ROL'* | Bank angle | ° | 100 Hz |
| *'ADAHRS_ARI_ARR_PIT'* | Pitch rate | °/s | 100 Hz |
| *'ADAHRS_ARI_ARR_ROL'* | Roll rate | °/s | 100 Hz |
| *'ADAHRS_ARI_ARR_YAW'* | Yaw rate | °/s | 100 Hz |

Table A.1.1: ADAHRS signals

| Channel name | Signal | Unit | Sample rate |
|---|---|---|---|
| *'ESIS_ARI_ANG_PITCH'* | Pitch angle | ° | 41.67 Hz |
| *'ESIS_ARI_ANG_ROLL'* | Bank angle | ° | 41.67 Hz |
| *'ESIS_ARI_ANG_MAGHEAD'* | Heading (magn.) | ° | 41.67 Hz |
| *'ESIS_ARI_LABEL_326_RAW'* | Pitch rate | °/s | 83.33 Hz |
| *'ESIS_ARI_LABEL_327_RAW'* | Roll rate | °/s | 83.33 Hz |
| *'ESIS_ARI_LABEL_330_RAW'* | Yaw rate | °/s | 83.33 Hz |
| *'ESIS_ARI_LABEL_331_RAW'* | Long. accel. | $m/s^2$ | 83.33 Hz |
| *'ESIS_ARI_LABEL_333_RAW'* | Lat. accel. | $m/s^2$ | 83.33 Hz |

Table A.1.2: ESIS signals

| Channel name | Signal | Unit | Sample rate |
|---|---|---|---|
| *'GIA1_ARI_LABEL_324_RAW'* | Pitch angle | ° | 20 Hz |
| *'GIA1_ARI_LABEL_325_RAW'* | Roll angle | ° | 20 Hz |
| *'GIA2_ARI_DST_RADALT'* | Altitude (radar) | ft | 10 Hz |
| *'GIA2_ARI_LABEL_103_RAW'* | Heading (GNSS) | ° | 10 Hz |
| *'GIA2_ARI_LABEL_313_RAW'* | Heading | ° | 10 Hz |
| *'GIA2_ARI_LABEL_315_RAW'* | Wind speed | m/s | 10 Hz |
| *'GIA2_ARI_LABEL_316_RAW'* | Wind angle | ° | 10 Hz |
| *'GIA2_ARI_LABEL_324_RAW'* | Pitch angle | ° | 10 Hz |
| *'GIA2_ARI_LABEL_325_RAW'* | Roll angle | ° | 10 Hz |
| *'GIA2_ARI_LABEL_326_RAW'* | Pitch rate | °/s | 10 Hz |
| *'GIA2_ARI_LABEL_327_RAW'* | Roll rate | °/s | 10 Hz |
| *'GIA2_ARI_LABEL_331_RAW'* | Long. accel. | g | 10 Hz |
| *'GIA2_ARI_LABEL_332_RAW'* | Lat. accel. | g | 10 Hz |
| *'GIA2_ARI_LABEL_333_RAW'* | Vert. accel. | g | 10 Hz |

Table A.1.3: Garmin signals

## A.2 Bank-to-bank rolls

FPR was also tried for bank-to-bank rolls but without success. The manoeuvre usually starts at values of $\phi$ up to 30° or 45°, the pilot then inputs lateral cyclic and a constant roll rate is achieved, the roll is stopped once the opposite extreme in bank angle is reached. The model fails to properly reconstruct this type of manoeuvre and both AoA and AoS fit are inadequate (figure A.2.1). A correlation between high bank angles and $\beta$ divergence can be spotted, this issue will be investigated in the future when more data will be available.

| Channel name | Signal | Unit | Sample rate |
|---|---|---|---|
| 'NB_ARI_ALT_HBARO' | Corr. barometric altitude | m | 50 Hz |
| 'NB_ARI_ALT_HP' | Pressure altitude | m | 50 Hz |
| 'NB_ARI_ALT_HP_COR_CALC' | Corr. pressure altitude | m | 50 Hz |
| 'NB_ARI_ANG_AOA' | Angle of Attack (AoA) | ° | 50 Hz |
| 'NB_ARI_ANG_AOA_COR_CALC' | Corr. angle of attack | ° | 50 Hz |
| 'NB_ARI_ANG_AOS' | Angle of Sideslip (AoS) | ° | 50 Hz |
| 'NB_ARI_PRS_PS' | Static pressure | hPa | 50 Hz |
| 'NB_ARI_PRS_PS_COR_CALC' | Corr. static pressure | hPa | 50 Hz |
| 'NB_ARI_PRS_PT' | Total pressure | hPa | 50 Hz |
| 'NB_ARI_PRS_QC' | Dynamic pressure | hPa | 50 Hz |
| 'NB_ARI_PRS_DP_AOA' | Differential pressure (AoA) | hPa | 50 Hz |
| 'NB_ARI_PRS_DP_AOS' | Differential pressure (AoS) | hPa | 50 Hz |
| 'NB_ARI_VEL_TAS' | True Air Speed (TAS) | m/s | 50 Hz |
| 'NB_ARI_VEL_TAS_COR_CALC' | Corr. TAS | m/s | 50 Hz |
| 'NB_ARI_VEL_CAS' | Calibrated Air Speed (CAS) | m/s | 50 Hz |
| 'NB_ARI_VEL_CAS_COR_CALC' | Corr. CAS | m/s | 50 Hz |
| 'NB_ARI_VEL_MACH' | Mach | - | 50 Hz |
| 'NB_ARI_VEL_ROC' | Rate of Climb | m/s | 50 Hz |
| 'NB_ARI_TMP_IAT' | Indicated air temperature | °C | 50 Hz |
| 'NB_ARI_TMP_SAT' | Static air temperature | °C | 50 Hz |
| 'NB_ARI_TMP_TAT' | Total air temperature | °C | 50 Hz |

Table A.1.4: Noseboom signals

## A.3 Other error models

At first, the error model in the linear accelerations was not considered, in this case, TAS matching is significantly worse (figure A.3.1).

Another try was made using a different error model for $\alpha$:

$$\alpha_{\mathrm{m}} = K_{\alpha}\alpha_{\mathrm{c}} + b_{\alpha} + K_{\alpha_{\beta}}\beta_{\mathrm{c}} \tag{A.16}$$

the reconstruction (figure A.3.2 and A.3.3) was overall worse than the model shown in chapter 5. Parameters values are shown in table A.3.1.

| Channel name | Signal | Unit | Sample rate |
|---|---|---|---|
| 'HC_MAS_TOT_CALC' | Weight | kg | 32 Hz |
| 'HC_CG_X_LAT_CALC' | CoG lat. coord. | m | 32 Hz |
| 'HC_CG_Y_LNG_CALC' | CoG long. coord. | m | 32 Hz |
| 'HC_CG_Z_VERT_CALC' | CoG vert. coord. | m | 32 Hz |
| 'HC_MOI_IXX_CALC' | MoI long. axis | $\mathrm{kg\,m^2}$ | 32 Hz |
| 'HC_MOI_IYY_CALC' | MoI lat. axis | $\mathrm{kg\,m^2}$ | 32 Hz |
| 'HC_MOI_IZZ_CALC' | MoI vert. axis | $\mathrm{kg\,m^2}$ | 32 Hz |
| 'HC_POI_IYZ_CALC' | PoI (YZ) | $\mathrm{kg\,m^2}$ | 32 Hz |
| 'HC_POI_IXZ_CALC' | PoI (XZ) | $\mathrm{kg\,m^2}$ | 32 Hz |
| 'HC_POI_IXY_CALC' | PoI (XY) | $\mathrm{kg\,m^2}$ | 32 Hz |

Table A.1.5: Weight and balance signals

| Channel name | Signal | Unit | Sample rate |
|---|---|---|---|
| 'CNT_ANG_COL' | Collective deflection | % | 64 Hz |
| 'CNT_ANG_CYCLIC_LAT' | Lat. cyclic deflection | % | 64 Hz |
| 'CNT_ANG_CYCLIC_LNG' | Long. cyclic deflection | % | 64 Hz |
| 'CNT_ANG_PED' | Pedal deflection | % | 64 Hz |

Table A.1.6: Control inputs signals

| Parameter | Value |
|---|---|
| $b_\alpha$ | -1.6517° |
| $K_\alpha$ | 0.983 |
| $K_{\alpha_\beta}$ | 0.034 |
| $b_\beta$ | -4.584° |
| $K_\beta$ | 0.324 |
| $b_{\bar{q}}$ | 0.08 Pa |
| $K_{\bar{q}}$ | 0.797 |

Table A.3.1: Error model parameters, with $K_{\alpha_\beta}$

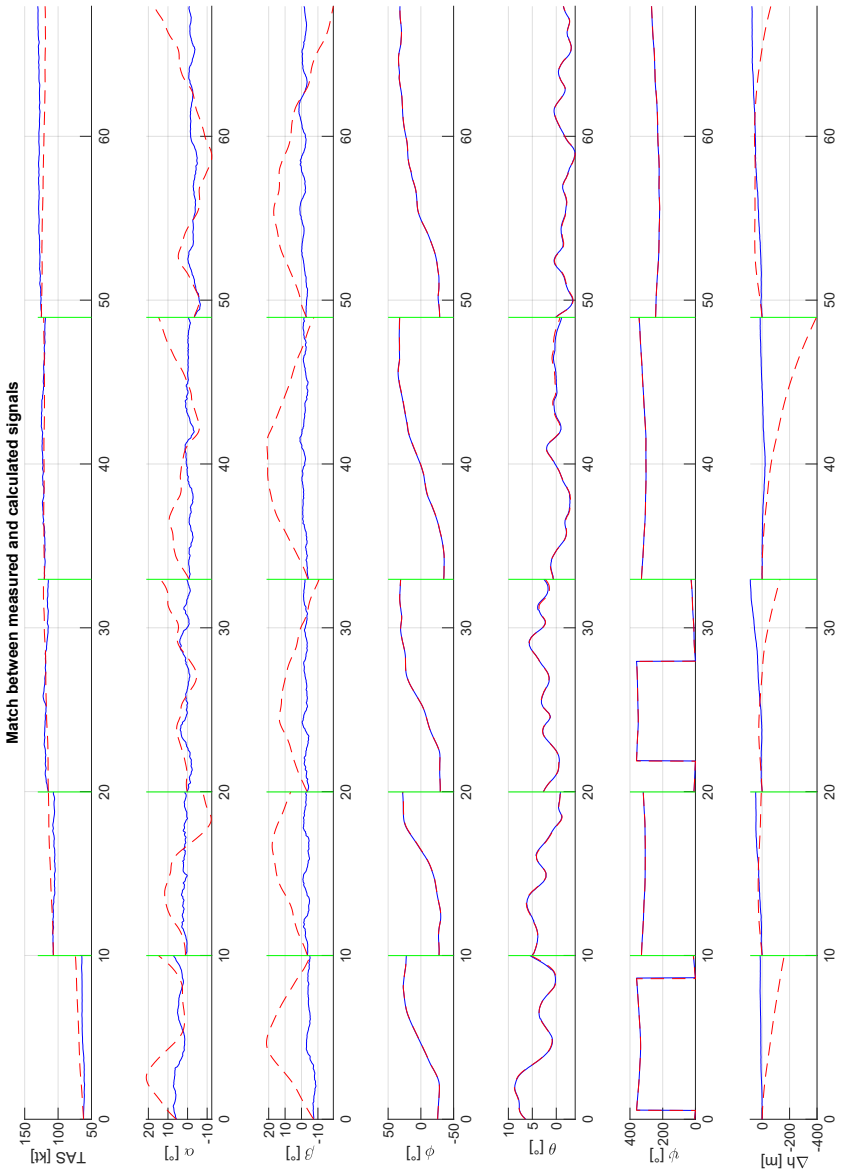


Figure A.2.1: Matching plot for bank-to-banks, blue: meas., red: recon.

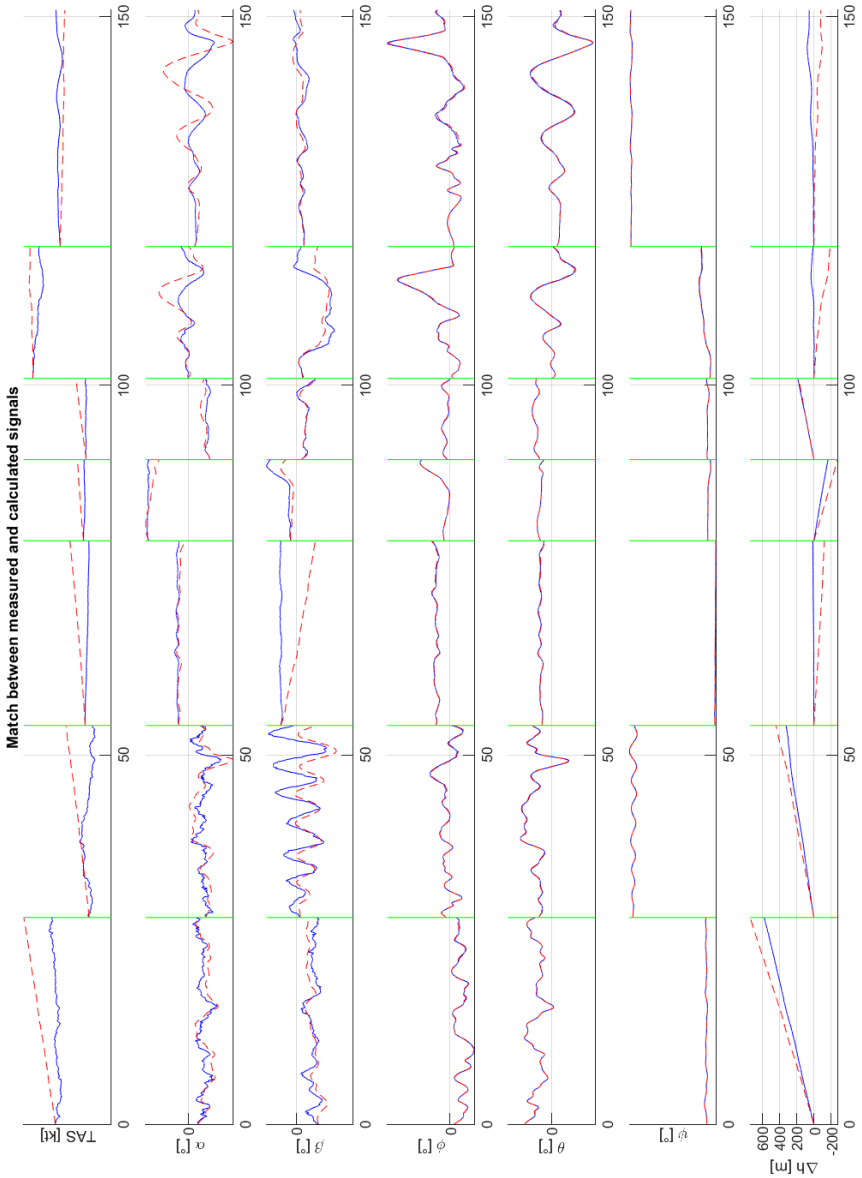


Figure A.3.1: Matching plot without accelerometer error model, blue: meas., red: recon.

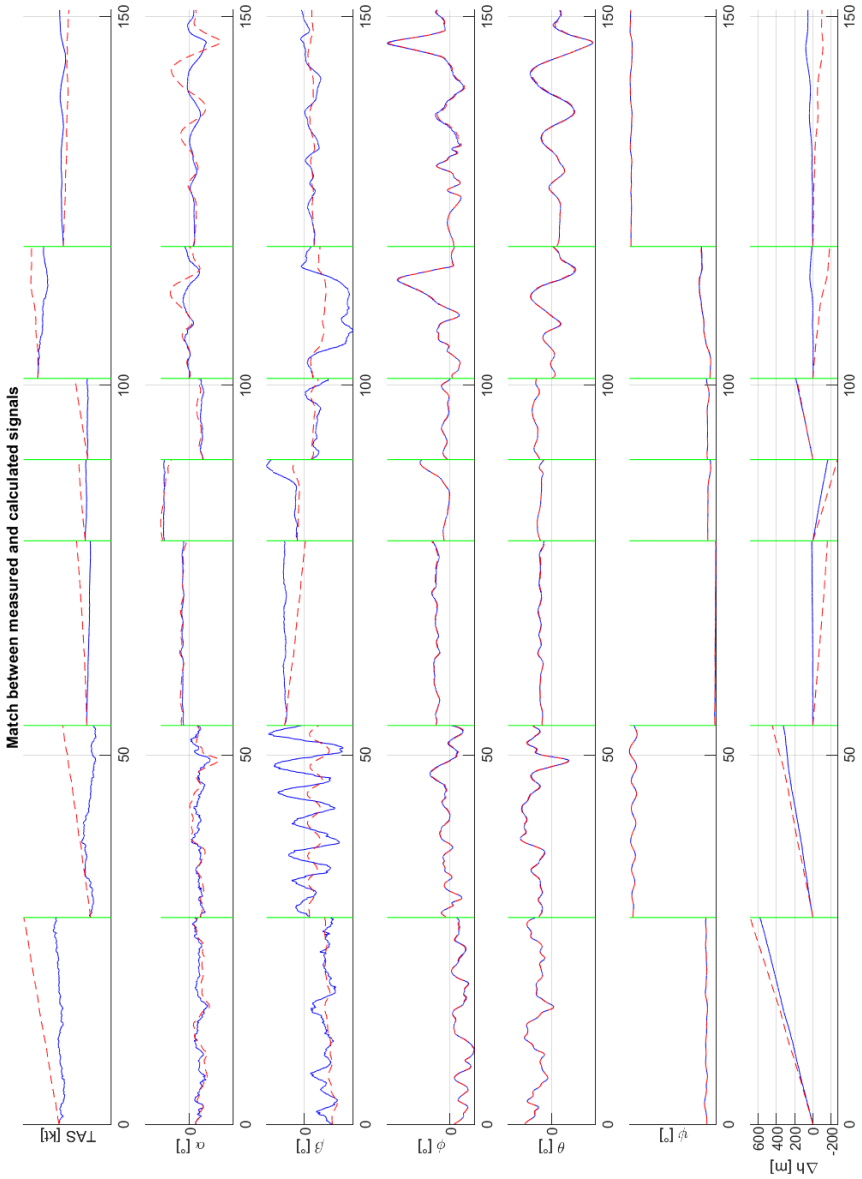


Figure A.3.2: Matching plot with different error model, blue: meas., red: recon.

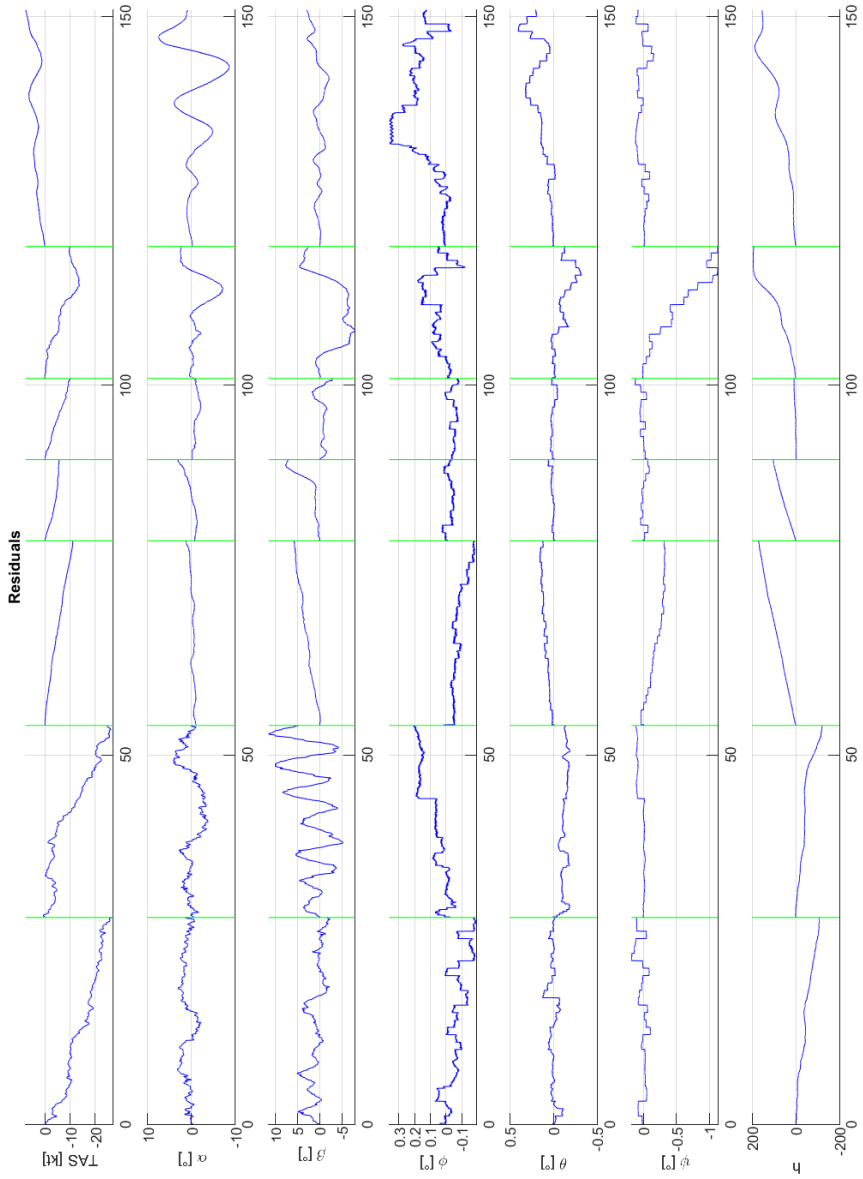


Figure A.3.3: Residuals plot with different error model

# Bibliography


[1] J. R. Schiess V. Klein. *Compatibility Check of Measured Aircraft Responses using Kinematic Equations and Extended Kalman Filter*. Tech. rep. Langley Research Center, NASA, 1977.

[2] Ravindra V. Jategaonkar. *Flight Vehicle System Identification: A Time Domain Methodology*. American Institute of Aeronautics and Astronautics, 2006.

[3] Jan Juraj Deverlija. "Aerodynamic Model Development For General Aviation Aircraft Based On Flight Test Data". Master's Thesis. University of Zagreb, 2021.

[4] David Haber-Zelanto. "Aerodynamic coefficients estimation of a general aviation airplane from flight test data". Master's Thesis. University of Zagreb, 2021.

[5] Advisory Group for Aerospace Research and Development. *Rotorcraft System Identification*. Tech. rep. AGARD, 1991.

[6] Gareth D. Padfield. *Helicopter Flight Dynamics*. Wiley, 2018.

[7] Airlines Electronic Engineering Committee. *Arinc Specification 429*. Tech. rep. Aeronautical Radio, Inc., 2004.

[8] Christian Raab. "Practical examples for the flight data compatibility check". In: *CEAS Aeronautical Journal* (2023).

# Sitography


[9] ZHAW. *WHeSI White-box Helicopter System Identification*. https://www.zhaw.ch/en/engineering/institutes-centres/zav/air-vehicle-design-and-technology/flight-mechanics-and-flight-control-systems/whesi/.

[10] Kopter. *AW09*. https://koptergroup.com/sh09/.

[11] Leonardo. *AW09*. https://helicopters.leonardo.com/en/products/aw09.

[12] National Instruments. *Test and Measurement Systems, a part of Emerson - NI*. https://www.ni.com/en.html.